METEOROLOGICAL OVERVIEW OF THE DEVASTATING 27 APRIL 2011 TORNADO OUTBREAK

BY KEVIN R. KNUPP, TODD A. MURPHY, TIMOTHY A. COLEMAN, RYAN A. WADE, STEPHANIE A. MULLINS, CHRISTOPHER J. SCHULTZ, ELISE V. SCHULTZ, LAWRENCE CAREY, ADAM SHERRER, EUGENE W. MCCAUL JR., BRIAN CARCIONE, STEPHEN LATIMER, ANDY KULA, KEVIN LAWS, PATRICK T. MARSH, AND KIM KLOCKOW

The outbreak of 199 tornadoes on 27 April 2011, the most significant since the dawn of reliable records, was generated by parent storm systems ranging from quasi-linear convective systems to long-lived discrete supercell storms.

A large number of tornadoes were recorded during the spring 2011 season, particularly a record number (around 758) during the month of April (NOAA 2011; NOAA 2012; Simmons and Sutter 2012a,b). A few tornado outbreaks accounted for the majority of the most damaging and lethal tornadoes, including extended outbreaks on 14–16 April [about 170 tornadoes, mostly EF-0 to EF-2 on the enhanced Fujita (EF) scale over primarily three regions: Oklahoma (OK)–Arkansas (AR), southern Mississippi (MS)/Alabama (AL), and the mid-Atlantic] and 25–28 April from Texas (TX) to eastern Virginia (VA) (~350 tornadoes, 321 fatalities) and 1-day outbreaks on 22 May [~48 tornadoes from OK to Wisconsin (WI), including the lethal EF-5 tornado in Joplin, Missouri (MO)] and 24 May [~47 tornadoes in Kansas (KS), OK, AR, and TX, including one EF-5 in OK].

In this overview paper, we summarize the tornado super outbreak of 27 April 2011, defined herein as the 24-h period midnight–midnight central daylight time (CDT) (0500 UTC). By many metrics this disastrous outbreak exceeds the super outbreak of 3–4 April 1974 (Fujita 1974; Corfidi et al. 2010). The number of tornadoes over a 24-h period for the 27 April 2011 outbreak was 199 (Fig. 1); tornado fatalities were 316 (the most in a 24-h period since 21 March 1932; NOAA 2011), and injuries exceeded 2,700. For the month of April, insurable losses from tornadoes surpassed $11 billion (U.S. dollars), while the total loss is estimated at around $15.5 billion (Simmons et al. 2012). The super outbreak on 27 April accounted for the majority of these losses. The amount of debris produced by the 27 April outbreak was staggering,

AFFILIATIONS: KNUPP, MURPHY, COLEMAN, WADE, MULLINS, C. J. SCHULTZ, E. V. SCHULTZ, CAREY, AND SHERRER—University of Alabama in Huntsville, Huntsville, Alabama; MCCAUL—Universities Space Research Association, Columbia, Maryland; CARCIONE, LATIMER, AND KULA—National Weather Service, Huntsville, Alabama; LAWS—National Weather Service, Birmingham, Alabama; MARSH—Cooperative Institute for Mesoscale Meteorological Studies/National Severe Storms Laboratory, Norman, Oklahoma; KLOCKOW—University of Oklahoma, Norman, Oklahoma
CORRESPONDING AUTHOR: Dr. Kevin Knupp, University of Alabama in Huntsville, 320 Sparkman Drive, Huntsville, AL 35805
E-mail: kevin@nsstc.uah.edu

The abstract for this article can be found in this issue, following the table of contents.
DOI:10.1175/BAMS-D-11-00229.1

A supplement to this article is available online (10.1175/BAMS-D-11-00229.2)

In final form 21 August 2013

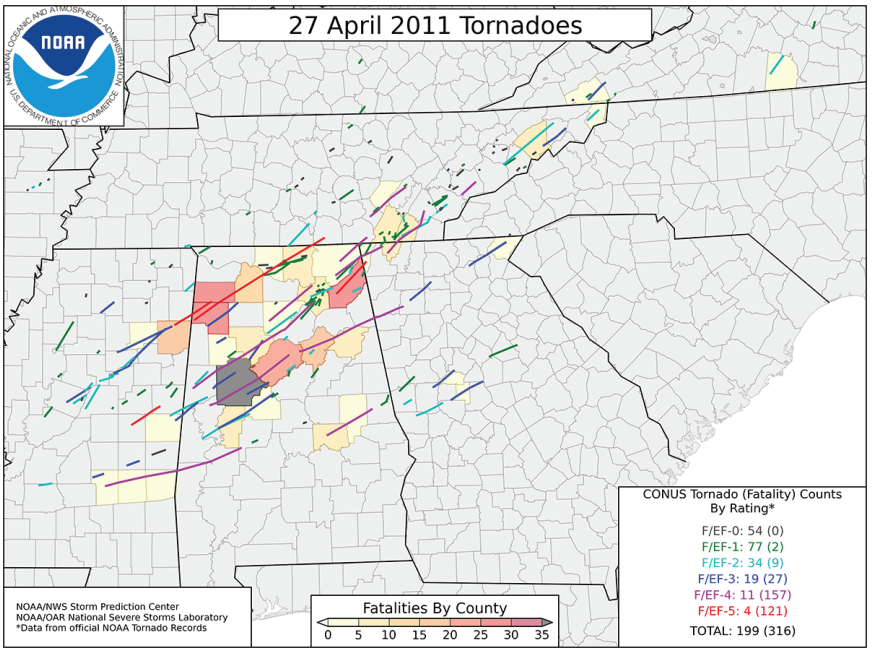

Fig. 1. Map of tornado paths on calendar day 27 Apr 2011. Tornado EF scale is color coded according to the scale given in the bottom right. Fatalities are given for each county according to the color scale in the bottom (center). Tornadoes continued over the Carolinas, northern Virginia, Indiana, Ohio, Pennsylvania, Maryland, and New York on 28 Apr.

with media-reported estimates of 10 million cubic yards (Birmingham News 2011).[1]

The 27 April tornado outbreak was the major component of an extended 4-day episode of tornadoes starting on 25 April and ending on 28 April. On 25 April, around 64 tornadoes (only four were EF-2 or greater intensity) were spawned between northeast TX and western Tennessee (TN) and Kentucky (KY). On 26 April, approximately 50 tornadoes were documented from eastern TX to the western portions of TN and KY. After the catastrophic outbreak on 27 April, the residual synoptic-scale system produced 43 additional tornadoes (four EF-2 and one deadly EF-3) from Georgia (GA) to New York (NY).

A primary motivation for this paper is to document the mesoscale and storm-scale characteristics of this outbreak, describe unique datasets, and present some initial analyses that are deemed worthy of more detailed investigations. Because numerous special datasets were acquired near the geographical core of this outbreak, we are compelled to describe some initial results without showing many details due to the space limitations of this article. Additional details and figures, including radar animations and soundings, are provided in the supplemental information of this paper (available online at http://dx.doi.org/10.1175/BAMS-D-11-00229.2).

This paper includes a meteorological overview of this outbreak and illustrates some unique features of three distinct episodes of tornadoes over this 24-h period (0500 UTC 27 April to 0500 UTC 28 April): 1) a mesoscale convective system (MCS) that evolved to an intense quasi-linear convective system (QLCS) during the early morning hours, 2) a smaller QLCS over northern AL during the midday hours, and 3) widespread discrete supercell storms during the afternoon–evening time period. We present a look at the environment(s) that supported these three rounds of severe weather, discuss some details and early analyses of each sequence, and mention projects related to the event, including some investigations that are not purely meteorological. Characteristics of these episodes are documented by Weather Surveillance Radar-1988 Dopplers (WSR-88Ds), a mix of surface measurements, ground surveys, and instruments operated by the University of Alabama in Huntsville (UAH), including the Advanced Radar for Meteorological and Operational Research (ARMOR) C-band dual-polarization radar, the Mobile Alabama X-band (MAX) dual-polarization radar, and the Mobile Integrated Profiling System (MIPS).

A variety of initial analyses have been conducted and brief summaries of the more interesting aspects are reported herein. Some of the more intriguing aspects of this outbreak include the following:

- Multiple modes of convective organization, including QLCSs, mesovortices embedded within the QLCSs, and discrete supercell storms (some associated with a thermal boundary) occurred during the outbreak.
- An impressive mesoscale vortex spawned within the early morning QLCS was associated with the

[1] Since trees are numerous in the southeast, tornadoes in this outbreak destroyed perhaps millions of trees.

rapid development of 16 tornadoes over north-central to northeast AL.
- The parent storms, including supercell storms and strong convective elements within QLCSs, were efficient in producing tornadoes. For example, about 90% of the supercell storms within the outbreak region produced at least one tornado.
- Many tornadoes were long tracked, wide, and intense.
- Analysis of polarimetric variables, combined with dual-Doppler analyses of a supercell storm, graphically illustrate that debris was effectively lofted to relatively high altitudes.
- Many of the violent tornadoes exhibited horizontal vortices along their periphery.
- External influences, including a thermal boundary, possible gravity waves, and topography, appeared to play a role in tornadogenesis and tornado intensity change.
- Despite timely and accurate warnings by the National Weather Service (NWS) forecast offices, the number of fatalities (316) was high.

The environment described in the following section was extremely conducive to the development of strong, long-track tornadoes. Although this dangerous situation was anticipated exceptionally well by the National Oceanic and Atmospheric Administration (NOAA) Storm Prediction Center (SPC), this paper does not focus on the forecasting aspects of this event, which are expected to be documented elsewhere.

THE SYNOPTIC AND MESOSCALE ENVIRONMENT OF THE OUTBREAK. This section presents an analysis of the environmental parameters highly conducive for tornadoes throughout the day across much of the region affected. We begin with the early component of the event. The environment during the early morning (0500–1200 UTC) QLCS tornado outbreak was characterized by appreciable low-level wind shear and modest CAPE values (~1000 J kg^{-1}) over northern and central MS and AL. The 0–1-km storm-relative helicity (SRH) values were prodigious, ranging from 500 to 700 m^2 s^{-2}. The 0–6-km bulk shear, around 25 m s^{-1}, was not extreme. However, the large low-level SRH was sufficient (Rasmussen 2003; Thompson et al. 2012) to produce numerous rotating updrafts and significant tornadoes along the QLCS.

In contrast, the environment over the region during the afternoon supercell outbreak was one of the most conducive to violent tornadoes ever documented in the literature. At 2200 UTC, the axis of a deep, negatively tilted upper-level trough was located over AR and Louisiana (LA). At 300 hPa, a 50 m s^{-1} jet extended around the base of the trough, from the Rockies into western AL (Fig. 2a). Positive differential vorticity advection at 500 hPa (DPVA; Fig. 2b) was present from AR into northern AL as air parcels exited the sharply curved upper trough. Paired with negligible thermal advection, the resulting net mass divergence within the column was associated with rapid surface pressure falls and associated isallobaric flow into a surface cyclone (995-hPa central pressure) centered in western KY at 2200 UTC (Figs. 2c,d), consistent with patterns documented in previous significant tornado outbreaks (Mercer et al. 2012). A strong surface cold front extended from the cyclone center in western KY into central LA at 2200 UTC. The rapid low-level height falls east of the trough axis in western KY contributed to a 30 m s^{-1} south-southwesterly low-level jet at 850 hPa over AL (Fig. 2c). The rapid height and surface pressure falls promoted ageostrophic flow within the lower boundary layer (Fig. 2d), where friction played an additional role in backing surface wind vectors at angles approximately 60° to the isobars, maintaining SRH values > 500 m^2 s^{-2} over the outbreak region.

The upper-level divergence and associated vertical motion helped promote steep lapse rates of 7.5°C km^{-1} between 700 and 300 hPa, according to the 2100 UTC North American Mesoscale Model (NAM) sounding at Cullman (north central), AL (Fig. 2h). The southerly flow at low levels transported warm and moist air northward from the Gulf of Mexico into central AL, where surface temperatures and dewpoints reached 25°–27°C and 19°–22°C, respectively, by 2200 UTC. This high-valued θ_e boundary layer air, along with cold temperatures and steep lapse rates aloft, produced CAPE values of 2500–3000 J kg^{-1} over central AL (Fig. 2e). Furthermore, the high surface dewpoints (Fig. 2h) produced a low-lifting condensation level (LCL), a measure that has shown some skill in differentiating tornadic and nontornadic supercell environments (e.g., Thompson et al. 2003). For example, just before the tornadic supercell moved over Tuscaloosa at 2200 UTC, the nearest Automated Surface Observing System (ASOS) station (KTCL) recorded a dewpoint depression of 4°C, producing an LCL height of 400–500 m AGL, in the 98th percentile for low LCLs in all supercell proximity environments according to the database assembled by Thompson et al. (2007, hereafter referred to as T07).

The strong upper-level trough and associated low-level height falls aided the production of a strong low-level wind field with extreme vertical wind shear as

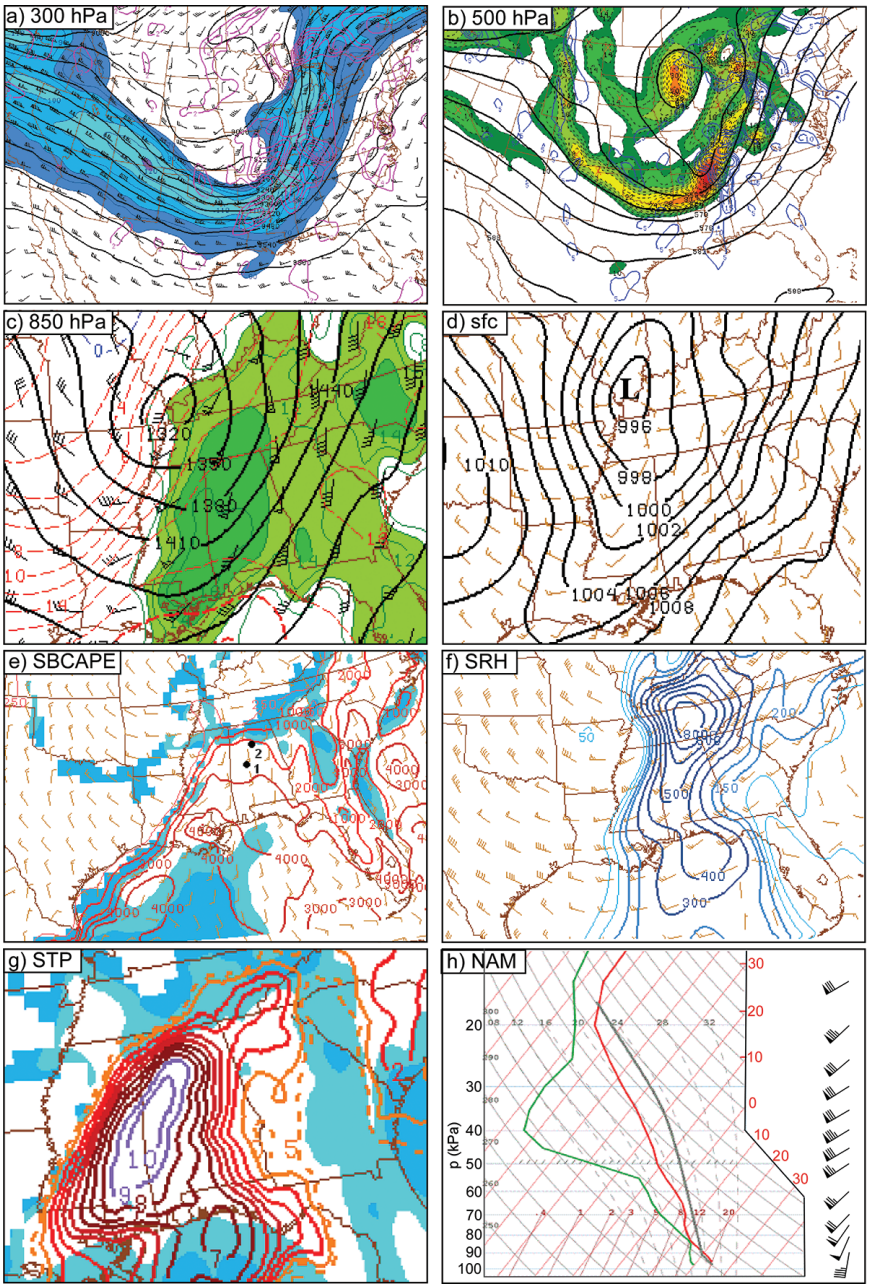

Fig. 2. (a) 300-hPa geopotential heights (m MSL, dark contours), isotachs [knots (kt); 1 kt = 0.51 m s^{-1}; blue shades with light and dark blue represent wind speed greater than 50 and 100 kt, respectively], and divergence (10^{-5} s^{-1}, purple line contours); (b) 500-hPa heights (dam MSL, black contours), vorticity (10^{-5} s^{-1}, shaded), and DPVA (blue contours); (c) 850-hPa heights (m MSL, black contours), mixing ratio (shaded, with light and dark green shading representing values greater than 10 and 14 g kg^{-1}, respectively), temperature (dashed red lines), and wind barbs; (d) mean sea level pressure (hPa, black contours) and surface wind barbs; (e) surface-based CAPE (J kg^{-1}, red lines) and surface-based CIN (light and dark blue shading represent values greater and 25 and 100 J kg^{-1}), numbered dots represent location of 1) Tuscaloosa and 2) Cullman; (f) 0–1-km storm-relative helicity (m^2 s^{-2}); (g) effective-layer significant tornado parameter; and (h) NAM sounding for Cullman, AL, at 2100 UTC 27 Apr 2011. [(a)–(c) are for 2200 UTC, and (d)–(h) are for 2100 UTC. In each panel with wind barbs, a full barb represents 10 kt, and a flag is 50 kt.] (Courtesy of NOAA Storm Prediction Center).

indicated by 0–1-km SRH values between 600 and 900 m^2 s^{-2} over the northern half of AL (Fig. 2f). In addition, an east-to-west–oriented thermal boundary developed during the late morning and early afternoon hours over northern AL owing to the cold outflow air produced by a midday QLCS, followed by persistent clouds and rain showers that maintained this cool air mass over northern AL, while relatively high insolation heated much of central AL. This boundary intensified by midafternoon and likely produced a low-level thermally direct circulation that enhanced the vertical wind shear along it (e.g., increased southerly flow above the cool air and diminished southerly flow near the surface within the cool air).

The significant tornado parameter (STP), which includes CAPE, SRH, and the effect of a low LCL (T07), attained values > 5 over a relatively large region including northeastern MS, central to northern AL, and areas to the northeast. Such a large area of high values serves as a good discriminator for tornado outbreaks (Shafer et al. 2012). A maximum STP value > 10 was diagnosed in eastern MS and western AL at 2200 UTC (Fig. 2g). The median STP value in T07 for significant (EF-2 or greater) tornado environments was near 2.5. Only 5 of 835 supercell proximity soundings examined by T07 had an STP greater

Table 1. Rankings of the top five tornado outbreaks in terms of the DPI, the N2 parameter (see text for details), and fatalities. All numbers are based on the SPC database. Outbreaks prior to 1950 are not included.

Date	DPI*	Date	N2 parameter**	Date	U.S. fatalities
27 Apr 2011	21,980	27 Apr 2011	28.0	27 Apr 2011	316
24 Apr 2010	7,330	3 Apr 1974	25.1	3 Apr 1974	307
3 Apr 1974	6,830	11 Apr 1965	10.3	11 Apr 1965	305
11 Apr 1965	4,230	05 Feb 2008	8.8	21 Feb 1971	226
30 Apr 1954	3,870	26 Apr 2011	7.5	21 Mar 1952	218

* The DPI, defined in Thompson and Vescio (1998) and Doswell et al. (2006), is the tornado area (length times width) multiplied by the (E)F-scale plus 1. The definition of width changed from a mean value to the maximum value in 1994 and hence the DPI values after this date will be higher than those based on mean width.

** Defined in Shafer and Doswell (2010), updated numbers provided by Dr. C. Shafer.

than 10, placing this environment well above the 99th percentile for supercell storms. In a recent study, covering the 2003–11 period (including the 27 April outbreak), Thompson et al. (2012) show a mean STP of 8.9 for EF-4 to EF-5 tornadoes. Storms over the warm sector where boundary forcing appeared subtle were more discrete than those that evolved along the boundary, in general agreement with the observations presented in Dial et al. (2010). Bunkers et al. (2006a,b) have presented observational evidence that discrete supercell storms exhibit longer lifetimes.

OVERVIEW OF THE TORNADO OUTBREAK. Tracks of all tornadoes for the 24-h period 0500 UTC 27 April–0500 UTC 28 April (from midnight to midnight CDT) are plotted in Fig. 1 (details on the characteristics of each tornado are available online at http://vortex.nsstc.uah.edu/uahsevere/April27/27April_Timeline.pdf). The greatest concentration of tornadoes occurred within an area of about 230,000 km^2 covering portions of MS, central to northern AL, eastern TN, and northern GA. Strong to violent tornado numbers include 19 EF-3, 11 EF-4, and 4 EF-5 tornadoes. In comparison, the 3–4 April 1974 outbreak occurred over a domain about four times larger and produced 35 F-3, 24 F-4, and 6 F-5 tornadoes (Corfidi et al. 2010).

Table 1 presents other statistics obtained from the SPC database, including the destruction potential index (DPI; Thompson and Vescio 1998; Doswell et al. 2006), the N2 parameter[2] introduced by Doswell et al. (2006) and further expanded by Shafer and Doswell (2010), and tornado fatalities for the top five outbreaks in each category. The 27 April 2011 outbreak tops the list in all three metrics. Even though the 3–4 April 1974 outbreak had greater numbers of F-4 and F-5 tornadoes, the long-track lengths and wide swaths of many tornadoes in the 27 April 2011 outbreak account for a greater DPI and N2 parameter.[3] On a state basis (not shown), the 27 April 2011 event ranks AL first in fatalities (238), first in total area (1.06% of the area of AL was impacted by tornadoes), and first in DPI. Thus, by many metrics, the 27 April 2011 outbreak was the most significant tornado outbreak since official records were started in 1950. The 3 April 1974 and 27 April 2011 outbreaks are clearly separated from other outbreaks when combinations of parameters (e.g., N2) are used as a metric.

Figure 3 depicts a time series of tornadogenesis events per 30-min time interval over the outbreak area shown in Fig. 1. Tornadogenesis events were absent in only six 30-min time blocks over this 24-h period. Three episodes of tornado activity are apparent. The first 76 tornadoes occurred during the 0500–1500 UTC time frame and were associated with a strong MCS that intensified over MS and evolved into a QLCS during the early morning hours over AL. The peak near 0630 UTC (Fig. 3) corresponds to the growth of an MCS composed of five intense

[2] The N2 index was selected since it is based on 13 tornado parameters, with the highest weights given to total number of tornadoes, number of significant tornadoes, number of violent tornadoes, destructive potential index, and pathlength of all tornadoes. Refer to Shafer et al. (2012) for details.

[3] After 1994, the width in the SPC database was changed from mean to maximum width along the tornado damage path (Brooks 2004). Thus, the numbers that are based on the width, such as DPI, will have a high bias. Given the change in tornado width recording methodology, it should also be noted that the sum of F-scale times pathlength was slightly larger on 27 April 2011 than on 3 April 1974.

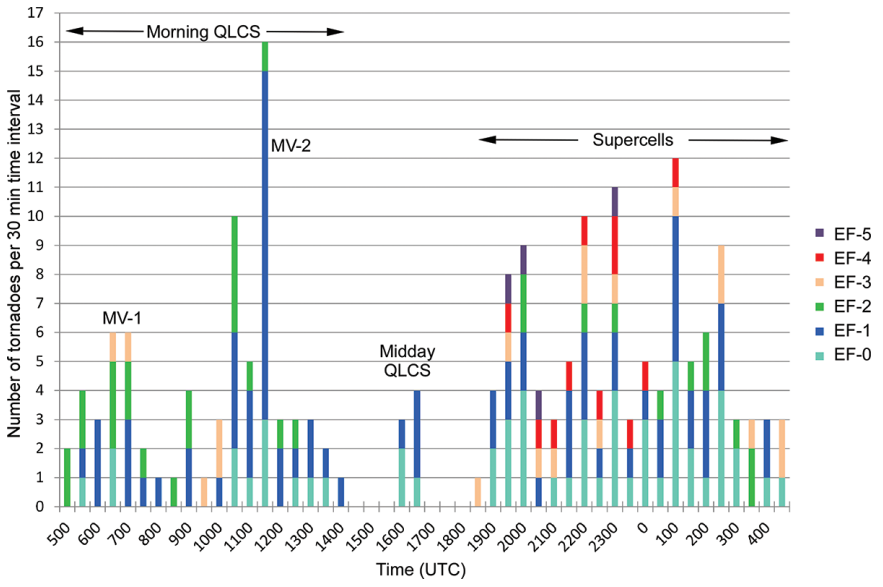

Fig. 3. Time series of tornadogenesis events per 30-min time interval.

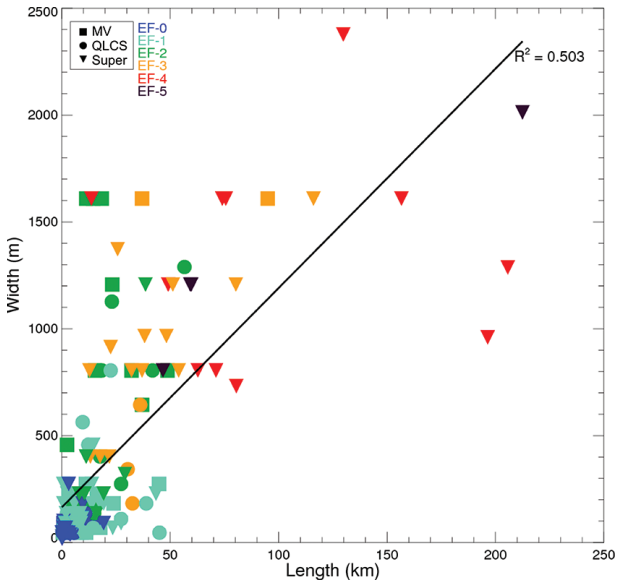

Fig. 4. Tornado width vs pathlength, stratified by EF scale and parent storm type (square for MV, circle for QLCS, and inverted triangle for supercell). A best-fit line is drawn and has a value (coefficient of determination) of $R^2 = 0.50$.

linear segments (each with length of ~100 km), one of which included a mesoscale vortex (MV; Trapp and Weisman 2003) over MS. The prominent peak near 1130 UTC (16 tornadoes within a 30-min period) was associated with the impressive development of a second, more notable MV over central and northeast AL, discussed in more detail in the following section.

A second, but shorter QLCS developed over northern AL around 1500 UTC, producing seven generally weak tornadoes (EF-0 and EF-1) between 1615 and 1705 UTC.

Finally, supercell storms formed over eastern MS and western AL during the afternoon hours, accounting for 29 of 34 tornadoes of EF-3 intensity or greater. The afternoon hours were very active, with an average of six tornadogenesis events per 30 min for the 7.5-h period between 1900 and 0230. The four EF-5 and 11 EF-4 tornadoes were initiated between 1930 and 0100 UTC; the formation of an EF-4 or EF-5 tornado was absent in only one 30-min period within this time interval.

The distributions of the EF scale, pathlength, and path width, all obtained from the SPC database, are plotted in Fig. 4. A modest correlation ($R^2 = 0.50$) between pathlength and path width (and tornado intensity) is suggested. There were 23 tornadoes that developed damage swaths greater than or equal to about 1 km, and 18 tornadoes had pathlengths exceeding 50 km (six exceeded a 100-km pathlength). The Hackleburg tornado over northern AL exhibited the longest path: about 212 km. Two other tornadoes were approximately 200 km in length. It is noteworthy that five EF-2 to EF-3 tornadoes within the morning QLCS produced damage path widths exceeding 1 km.

Primarily EF-3 and stronger tornadoes exhibited pathlengths exceeding 60 km, consistent with Brooks (2004). A broader range of tornado intensities (from EF-2 to EF-5) exhibited path widths exceeding 1 km. According to Brooks (2004, his Fig. 4) EF-2, EF-3, EF-4, and EF-5 tornadoes that achieve path widths greater than 1 km fall in the respective cumulative distribution function (CDF) values of approximately 99%, 95%, 90%, and 88%. Mean width values for EF-2 to EF-5 tornadoes (in the Brooks study) are 126, 264, 460, and 555 m, respectively.

OUTBREAK COMPONENTS AND CHARACTERISTICS. The following sections summarize the mesoscale and storm-scale features of three contrasting modes of mesoscale organization of deep convection that produced tornadoes during this outbreak.

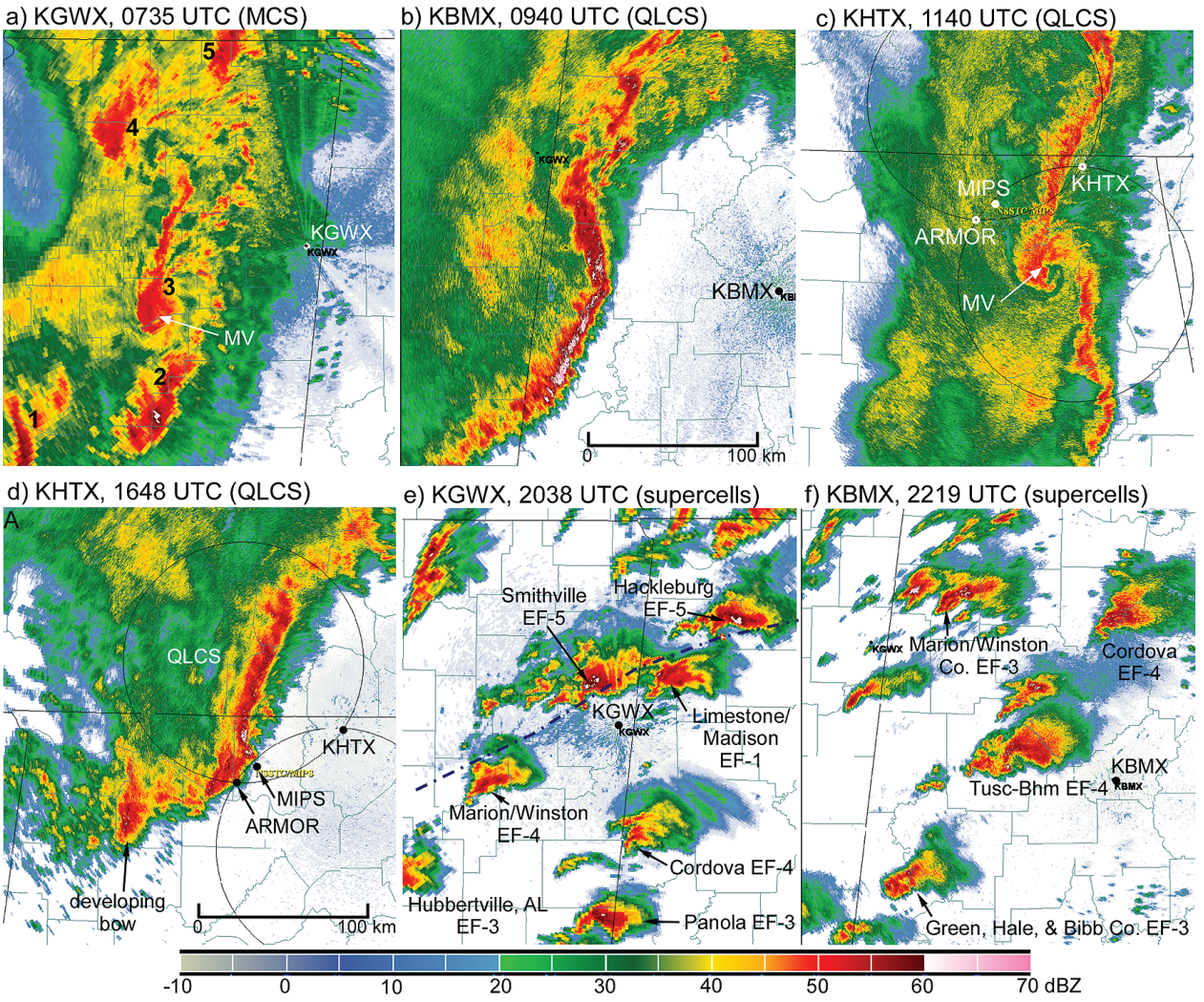

Fig. 5. Overview of the 27 Apr 2011 outbreak, showing the evolving MCS/QLCS during the (a)–(c) morning hours, (d) the midday QLCS, and (e),(f) supercell storms during the afternoon. All panels are the reflectivity factor at 0.5° elevation angle. The dotted–dashed line in (e) is the estimated location of the surface thermal boundary based on surface data.

Early morning QLCS. A large MCS formed over the LA–AR region and organized over MS around midnight CDT (0500 UTC) on 27 April. The QLCS was a vigorous system that generated an impressive 76 tornadoes, some of which exhibited EF-3 intensity, wide paths, and long tracks. Tornadogenesis events increased notably after 0500 UTC (Fig. 3) as this MCS intensified over MS and matured over AL (Figs. 5 a–c). Of the 76 tornadoes within the MCS/QLCS, 5 of them achieved EF-3 intensity. This number is unusually high when compared to the results of Trapp et al. (2005b), who found that EF-2 and stronger tornadoes are much less common within QLCSs relative to supercells. Their 3-yr dataset indicates a total of only 12 (E)F-3 tornadoes from QLCSs (see their Fig. 4). Grams et al. (2012) also show a relatively low number (22 during the 2000–08 period) of QLCS-generated tornadoes with intensities greater than or equal to EF-3 (see Fig. 2 in their paper).

An image from the Columbus, MS, WSR-88D (KGWX) at 0735 UTC (Fig. 5a) reveals five intense meso-β-scale components labeled 1–5. Component 3, which contained a mesoscale vortex (MV1), was the most prolific tornado producer, generating a series of eight tornadoes over a 60-min period, with two reaching EF-3 intensity, one of which produced a damage path 95 km in length. Six tornadoes produced damage path widths exceeding 1 km, which is much larger than typical tornado widths within QLCSs (Trapp et al. 2005b). Several tornadoes were associated with components 2, 4, and 5.

Component 1 rapidly expanded to form a bow echo after 0735 UTC, while the others merged into one contiguous QLCS that produced 31 tornadoes in

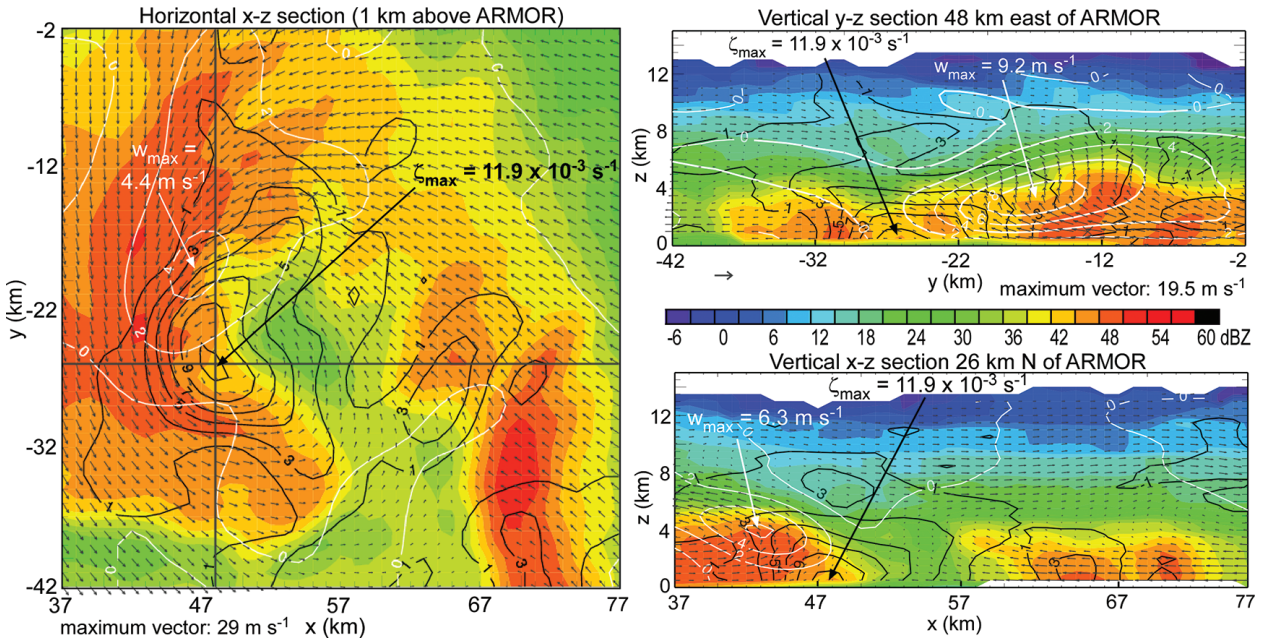

Fig. 6. Dual-Doppler analysis, using the ARMOR and KHTX radars, of the MV at 1145 UTC. Plan view at (left) 1.0-km level and (right) vertical sections along lines indicated in horizontal view. Vectors portray horizontal flow relative to the moving MCV. Contours are vorticity (solid black), plotted every 1 × 10^{-3} s^{-1} and vertical motion (solid white) plotted every 1 m s^{-1}.

central to northern AL. By 0940 UTC, a 200-km-long bow echo segment located over western AL (Fig. 5b) subsequently adjoined to the northern linear portion of the QLCS as the system moved into AL. This bow echo produced 10 of the 31 tornadoes within the entire QLCS over AL, 3 of which were significant EF-3 tornadoes, 2 with a track width > 1 km, and 4 (1) with a pathlength greater than 30 (50) km.

A second significant MV (MV2) formed within this QLCS by 1030 UTC. MV2 formed near the intersection of the bow echo with the linear segment to the north, similar to a tornadic MV examined by Schenkman et al. (2011a,b, 2012) and developed into one of the most striking components of this QLCS. The mature MV2 is shown in the 1140 UTC base elevation image of reflectivity factor (Z) from the Hytop, AL, WSR-88D (KHTX) in Fig. 5c. Tornadoes associated with MV2 are indicated as a distinct maximum in tornadogenesis events at 1130 UTC in Fig. 3. In AL, 18 tornadoes were associated with MV2, 3 of which achieved EF-2 intensity, while the others were estimated at EF-0 to EF-1. As MV2 moved to the northeast, it produced another EF-1 tornado in extreme northwest GA and three additional tornadoes (one each of EF-0, EF-1, and EF-2 strength) in southeast TN.

Since MV2 was located within a prime area of the dual-Doppler lobe formed by the KHTX and ARMOR radars (68-km baseline), a preliminary dual-Doppler analysis was conducted using standard techniques outlined in the online supplement. Figure 6 indicates that the horizontal flow relative to the translating MV is filled with positive vertical vorticity peaking at about 12 × 10^{-3} s^{-1} at the lowest analysis level of 1 km AGL. Based on initial results, we note the following apparent aspects of MV2: 1) it contained multiple vorticity centers at some analysis times; 2) cores of vertical vorticity from the northernmost convective cells along the attendant QLCS to the south advanced toward MV2 and merged with the primary vorticity area; 3) updrafts were shallow and relatively weak (<10 m s^{-1}) and their magnitudes peaked below 6-km height on the northern to western sides of the vortex; and 4) the storm-relative horizontal wind maximum migrated counterclockwise with time. These inceptive findings highlight the utility of a complete investigation of this MV and the potential mechanisms (e.g., Trapp and Weisman 2003; Weisman and Trapp 2003; Atkins and St. Laurent 2009) that allowed it to amplify and effectively produce tornadoes.

The vertical extent of significant precipitation (40-dBZ echo) within MV2 was mainly confined below 4–5 km, and the absence of lightning, as indicated by the National Aeronautics and Space Administration (NASA) Northern Alabama Lightning Mapping Array, corroborates the relatively weak and shallow dual-Doppler analyzed updraft. Yet, 12 tornadoes were rapidly produced over a 30-min period as MV2 moved over relatively rough topography. As was the case

for MV1 in MS, tornado production was relatively abundant within MV2 after an initial 30-km-long EF-3 tornado formed in west-central AL between 1018 and 1036 UTC. MV2 then produced a 48-km-long EF-2 tornado in Cullman County and then ramped up production of weaker tornadoes upon entering the more heterogeneous terrain of Marshall County. One possibility (hypothesis) is that variations in topography may have played a contributing role (perhaps in addition to the already well-primed environmental parameters discussed in the previous section) in the rapid increase in tornadogenesis events via topographic-induced stretching and channeling of flow (e.g., Bosart et al. 2006) within this relatively stable low-level environment that exhibited high values of vertical vorticity. Such a significant ramp-up in tornadogenesis is in contrast to the more gradual evolution of the parent MV.

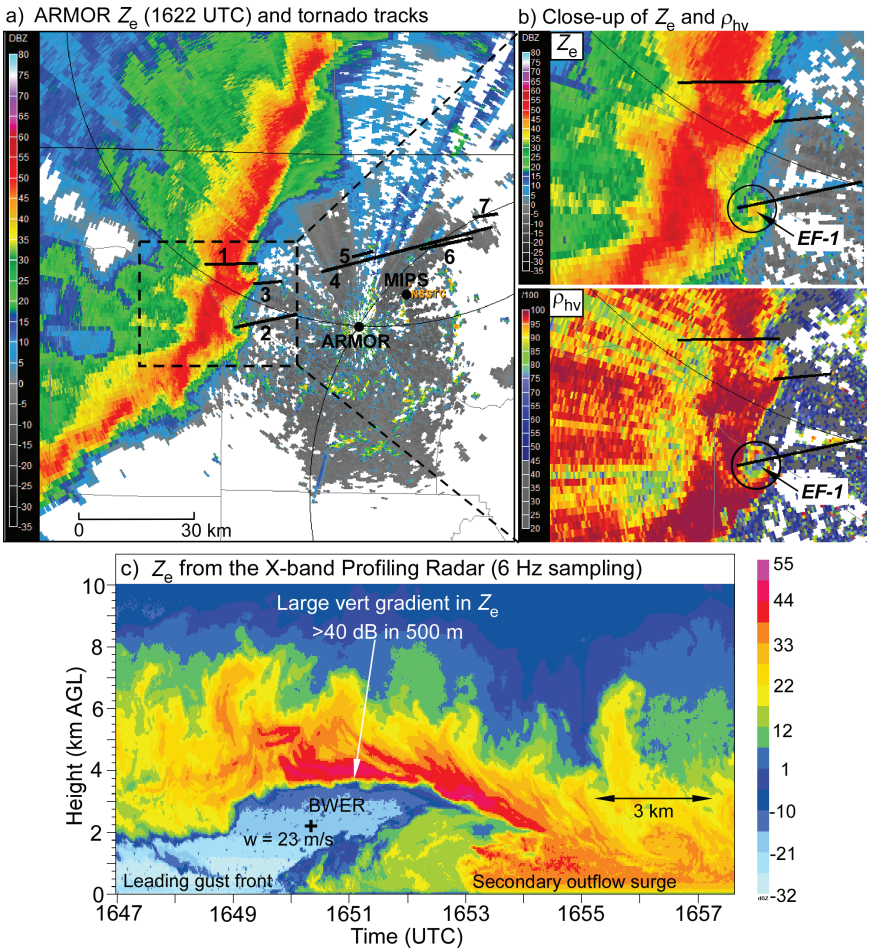

Fig. 7. (a) ARMOR image of equivalent reflectivity factor (Z_e) from the midday QLCS at 1622 UTC. The lines labeled 1–7 identify tornadoes associated with this QLCS. (b) Zoomed in view of well-defined curls in (top) Z_e, cyclonic circulations (circles), and tornadic debris signatures (circles) as indicated by (bottom) ρ_{hv}. (c) Time vs height section of Z_e from the MIPS XPR for the period 1647–1658 UTC. The maximum in vertical particle motion ($W = w + V_T$, where w is vertical motion and V_T is terminal fall speed) is annotated within the bounded weak echo region. See Fig. 5d for the MIPS location relative to the QLCS.

Midday QLCS over northern AL. A second, smaller (about 100 km in the north–south direction) QLCS formed as an intense convective line over northern MS and rotated from an initial east–west orientation at 1300 UTC to a south-southwest (SSW) to north-northeast (NNE) orientation by 1500 UTC as the system moved eastward. The QLCS front edge evolved from a linear and smooth structure at 1555 UTC to one that exhibited six protrusions in the Z field at 1615 UTC. These six protrusions appear to be associated with distinct inflow notches exhibiting an average horizontal separation of ~8.5 km. Each protrusion was associated with either a recent passage or the superposition of a reflectivity segment (RS[4]), oriented perpendicular to the QLCS passing along the axis of the QLCS from the southwest to northeast. By 1622 UTC, two of these protrusions had developed well-defined forward-flank curl structures (hooklike echoes) produced by cyclonic circulations that were associated with a sequence of seven EF-0 to EF-1 tornadoes as the QLCS moved over the UAH observational network in north-central AL

[4] A reflectivity segment is a quasi-linear feature in reflectivity factor that appears to play a role in tornadogenesis. The RS kinematic and dynamic features have not been defined previously, but we have observed a correlation between intersection of an RS with an existing supercell storm, and a subsequent increase in circulation, in other tornadogenesis events over northern Alabama (e.g., Coleman and Knupp 2008).

between 1615 and 1705 UTC. An image of Z from the ARMOR (Fig. 7a) shows curl structures at the leading edge at 1622 UTC when two tornadoes were in progress. Both of these primary curl structures exhibited dual-polarized tornadic debris signatures (i.e., reduction in correlation coefficient ρ_{hv}, as shown in the bottom panel of Fig. 7b; see Ryzhkov et al. 2005 and Schultz et al. 2012) at some point during their lifetime (Fig. 7b). Tornado paths associated with these signatures were verified by detailed ground surveys. The intense nature of the QLCS is further evidenced by peak Z values of 65 dBZ, cooling of 7.6 K, and peak wind gusts of 17.4 m s^{-1} at the UAH MIPS site and 26 m s^{-1} at the Huntsville airport ASOS surface station (KHSV), located at 237°, 16 km southwest of the MIPS.

Other special observations include a sounding just ahead of the QLCS at 1700 UTC from Redstone Arsenal, AL (RSA), measurements from the MAX radar 42 km northeast of the ARMOR, and the passage of the southern portion of the QLCS over the MIPS. Figure 7c shows a high-resolution time–height section of Z_e from the MIPS X-band (vertically pointing) Profiling Radar (XPR). The time scale in this figure was selected to form an approximate 1:1 correspondence between the vertical and horizontal scales using a time-to-space conversion and the observed storm motion. A vertical section reconstructed from the KHTX radar (not shown), located 50 km to the northeast, corroborated the structure and relative distribution of Z. The relative location of this section is shown in Fig. 5d. Annotated features include a bounded weak echo region filled with updraft and two outflow surges that correspond to wind surges in collocated surface measurements. Of particular importance is the peak 23 m s^{-1} updraft located at a relatively low level near 2 km, indicating that dynamic forcing near the nose of the initial outflow surge was likely prominent. The passage of a tornado ~9 km north of the MIPS/XPR site suggests that this updraft measurement is representative of the leading edge of the MCS where tornadogenesis occurred. Storm-relative helicity (0–3 km) values of 870 m^2 s^{-2} estimated from the 1700 UTC RSA sounding (> 1100 m^2 s^{-2} from the SPC mesoanalysis), significant cyclonic shear along the leading edge of the QLCS, and significant stretching as implied by the strong low-level updraft all combined to make a limited region of the QLCS efficient in producing tornadoes in this time–space window of the observations. Since the ARMOR was alternating between sector and 0.7° elevation surveillance scans, the temporal resolution at low levels is 1–2 min during the passage of the QLCS within close range of the ARMOR. The combined MIPS, ARMOR, and MAX observations will provide a basis for a comprehensive future study of tornadogenesis within this particular QLCS.

A second trailing line of intense deep convection developed around 1630 UTC rapidly evolved into a short bow echo segment (Fig. 5d) that produced wind damage across northern AL and eventually overtook and merged with the leading QLCS by 1800 UTC. As this combined QLCS propagated into northeast AL and southeast TN, it evolved to a cellular structure consisting of individual supercell storms that produced several tornadoes over southeastern TN. This evolution is similar to the slabular to cellular transformation within an intense derecho (bow echo) event described by Weisman et al. (2013).

It is noteworthy that the early morning and midday QLCS events produced significant local power outages from central to northern AL that significantly reduced warning dissemination (owing to power outages, disabled sirens, and reduced weather radio transmissions) to these areas during the more significant afternoon supercell-spawned tornadoes (TRAC 2012). Additionally, these systems laid the basis for an influential thermal boundary that appears to have aided in the strength of the northernmost afternoon supercells.

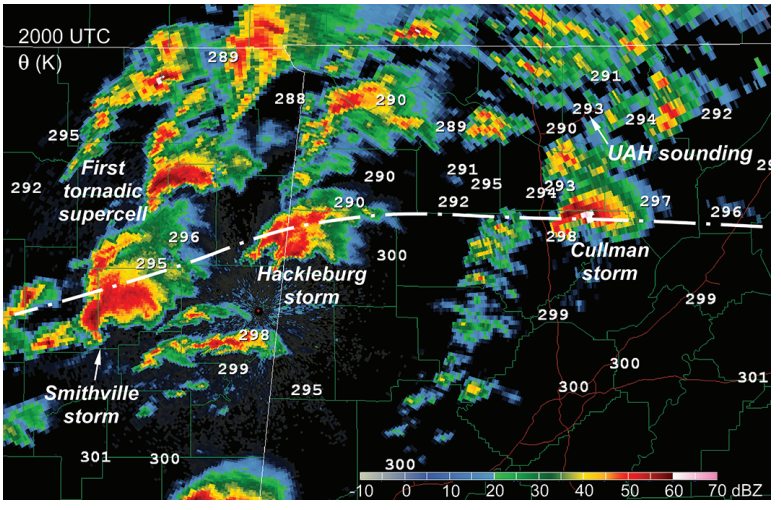

Fig. 8. Surface potential temperature (K) superimposed on reflectivity factor from the Columbus, MS (KGWX), WSR-88D. The radar image and surface values are valid for 2000 UTC. The thermal boundary is represented as a dotted–dashed line. The UAH sounding is shown in Fig. 9.

Characteristics of the thermal boundary. The thermal boundary produced by the midday QLCS and reinforced by subsequent overcast and scattered showers within the northern portion of the outbreak area was a prominent mesoscale feature. The potential importance of thermal boundaries has been investigated in previous studies (Davies et al. 1994; Markowski et al. 1998; Langmaid and Riordan 1998; Koch et al. 1998; Rasmussen et al. 2000; Thompson and Edwards 2000; Rogash and Smith 2000). Surface data from a variety of sources were used to estimate the time-resolved boundary location from the time of formation in the wake of the midday QLCS at 1500–1700 UTC through the afternoon hours. Potential temperature plotted in Fig. 8 shows the boundary extending from northeastern MS to northern AL at 2000 UTC. The horizontal temperature gradient varied along the boundary, ranging from about 6 K (22 km)$^{-1}$ [normalized gradient of about 3 K (10 km)$^{-1}$] obtained from a southward transect by a UAH mobile mesonet near the Cullman storm between 1959 and 2013 UTC to a 5-K increase over 20 min [5-km distance or a normalized gradient of 10 K (10 km)$^{-1}$, assuming a 4 m s^{-1} boundary speed toward the north] near the Hackleburg storm location in Fig. 8. The gradient in θ over northeastern MS is relatively diffuse. The vertical structure north of this boundary was sampled by the MIPS instrumentation and a special radiosonde released at 2052 UTC (Fig. 9) from the MIPS location annotated in Fig. 8. This sounding reveals a layer of cool air about 400 m deep, where potential temperature increased by 7 K over the lowest 400 m. The surface-based, lowest 100-mb mean layer and most unstable values of CAPE [convective inhibition (CIN)] were ~0 (–560), 1600 (–45), and 2700 (–5) J kg^{-1}, respectively.[5]

The boundary may have played a key role in convective initiation, and it interacted with several storms (discussed in the following section), including the Smithville, Hackleburg, and Cullman storms identified in Fig. 8. Moreover, the first supercell-spawned tornado (EF-3) initiated at 1836 UTC when the parent storm (annotated as "first tornadic supercell" in Fig. 8) was near this boundary over northeastern MS.

Supercell storms during the afternoon and evening. Discrete supercell storms formed near 1800 UTC in MS and AL as surface temperatures south of the boundary increased to around 26°C (299 K; Fig. 8). The initial echo shape of many supercell storms was an elongated crescent (RS, defined in footnote 5) with the major axis oriented west-northwest to east-southeast, approximately perpendicular to the low-level shear vector (not shown). Some of the incipient RSs intensified to supercell storms, while others did not evolve beyond these weaker RS formations. All violent EF-4 to EF-5 tornadoes, and many of the EF-3 tornadoes, were generated by supercell storms between 1836 UTC in northeast MS and 0541 UTC (28 April) in western Virginia. The fraction of supercell storms that produced tornadoes, about 90%, is unusually high (Trapp et al. 2005a[6]) but is consistent with the extremely high values of the EHI and STP parameters, both in the 99th percentile (T07).

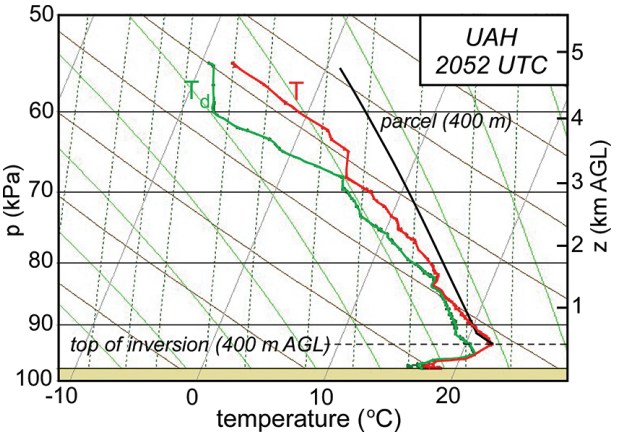

Fig. 9. Sounding acquired from UAH at 2052 UTC. The black solid line shows the path of a parcel ascending adiabatically from the top of the cold air pool. The sounding terminated near 55 kPa due to loss of signal.

Figures 5e and 5f show the field of supercell echoes sampled by the Columbus, MS (KGWX), and Birmingham, AL (KBMX), WSR-88Ds at 2038 and 2219 UTC, respectively, during the maximum time period for supercell tornadogenesis. Seven supercell storms are annotated at 2038 UTC:

1) A supercell that produced an EF-5 tornado was approaching Smithville, MS.
2) The Hackleburg storm was located just past Phil Campbell, AL, where an EF-5 tornado produced some of the most intense damage. Both the Smithville and Hackleburg EF-5 tornadoes were located near the thermal boundary (Fig. 8) whose position is shown as a dashed line in Fig. 5e.

[5] To calculate CAPE, the missing values above 500 mb of the sounding in Fig. 9 were filled in with values from the Redstone Arsenal sounding released at 1700 UTC from a location 14 km south of the UAH sounding site.

[6] The Trapp et al. (2005a) study examined the likelihood of tornadic mesocyclones as a function of the lowest detectable height.

3) South of the KGWX radar, the Cordova storm was a well-defined supercell just prior to genesis of the initial long-tracked (~200 km) EF-4 Cordova tornado.
4) The Limestone/Madison County supercell storm between the Smithville and Hackleburg storms produced an EF-2 tornado about 2 h after the time of this image.
5) The Marion/Winston supercell storm located west-southwest of KGWX produced an EF-3 tornado in Marion and Winston Counties in western AL at 2210 UTC.
6) The Panola supercell south of the Cordova storm produced an EF-3 tornado about 10 min after the time of this radar image.
7) The seventh supercell in the lower-left corner of Fig. 5e produced an EF-3 tornado near Hubbertville, AL, about 90 min after the time of this radar image.

Figure 5f shows four significant tornadic supercell storms at 2219 UTC:

1) The highly publicized Tuscaloosa–Birmingham (high end) EF-4 tornado (130-km length and 2.3-km maximum width) was in progress.
2) The Cordova EF-4 long-track tornado was also in progress.
3) The Marion–Winston EF-3 tornado (in progress, parent storm is also annotated in Fig. 5e) developed a track length and width of 52 and 1.2 km, respectively.
4) The Green–Hale–Bibb County storm, located southwest of KBMX, was within 11 min of forming an EF-3 tornado with an eventual 115-km track length and maximum width of 1.6 km.

The high efficiency of tornadogenesis is corroborated in Figs. 5e and 5f; with the exception of the Limestone/Madison County storm (Fig. 5e) that produced only one EF-2 tornado, every supercell within the domain of these figures produced at least one tornado of at least EF-3 intensity.

Table 2 presents statistics on three of the most proficient supercell storms, where proficiency is defined herein by the accumulative tornado pathlength divided by the total distance traveled by the parent storm. The Cordova storm persisted as a supercell storm for 9 h, traveling 850 km while producing nine tornadoes, including one EF-5, two EF-4s, and one EF-3. The Tuscaloosa–Birmingham storm was perhaps the most proficient (relative to the supercell storm pathlength), generating four tornadoes with an accumulated pathlength of 380 km, representing 52% of the storm track. The Cullman storm was the first supercell to form in AL and produced eight tornadoes during its 7-h lifetime as a supercell, three of which attained EF-4 intensity. This storm was observed by one of the authors (T. Coleman) when it presented supercell (rotational) characteristics 1.7 h after first echo.

A closer examination of three of the aforementioned significant storms and associated tornadoes further illustrates some important aspects of the structure of supercell storms and tornadoes within this outbreak. Figure 10 shows a dual-Doppler analysis of the Cullman storm at 2023 UTC and an image of the first of eight tornadoes generated by this storm. The intensity of the 1-km-wide tornado is near EF-4 at this time. This tornado, like others on this day, exhibits a tilt toward the direction of motion (northeast) due to the large translational speed of about 24 m s^{-1}. The horizontal storm-scale flow (Fig. 10b) shows

Table 2. Statistics on the most prolific supercell storms on 27 Apr 2011.

Storm ID	Time of first echo (UTC)	Start time, supercell phase* (UTC)	Time of first tornado (UTC)	End time, supercell phase (UTC)	Lifetime of supercell phase (h)	Pathlength of supercell phase (km)	No. of tornadoes	Accumulative tornado track (km) (proficiency, %)	Violent tornadoes
Cordova	1929	1956	2040	0500	9	850	9	415 (49)	1 EF-5, 2 EF-4, and 1 EF-3
Tuscaloosa	1829	2037	2143	0345	8	730	4	380 (52)	2 EF-4 and 2 EF-3
Cullman**	1709	1851	1940	0215	7	650	8	250 (38)	3 EF-4

* Start time of supercell phase is determined by radar criteria defined from the supercell nomogram from Andra (1997).

** The Cullman storm interacted with the boundary over northern AL, whereas the Tuscaloosa and Cordova storms were embedded within the more homogeneous warm sector.

a strong southeasterly inflow into the weak echo region east of the tornado, which is centered on the closed cyclonic circulation and debris ball (a circular region of high Z values; see Bodine et al. 2013) near $(x, y) = (25, -30)$. The dashed line in Fig. 10b indicates the location of vertical cross sections displayed in Figs. 10c and 10d. A tornadic debris signature, based on high values of Z and low values of the correlation coefficient (ρ_{hv}; see Ryzhkov et al. 2005; Bodine et al. 2013; Schultz et al. 2012), extended to heights of 4 km around this time (and up to 7 km at 10 min earlier at 2013 UTC), as shown by the black solid contours in Fig. 10d. The relation between the tornado location and the updraft core, shown in Figs. 10c and 10d, suggests an efficient transfer of debris from the tornado circulation to the primary storm updraft. In this case, the retrieved airflow could be used along with the debris signature to calculate trajectories and enhance the understanding of debris transport to long ranges, a common occurrence in violent tornadoes (Magsig and Snow 1998; Knox et al. 2013).

Figure 11 presents a visual image and radar images of the Hackleburg tornado and its parent storm approaching the small community of Tanner, AL, where high-end EF-4 damage occurred. Because the tornado is located within the cool, nearly saturated air north of the boundary, the low cloud base is around 200–300 m AGL and nearly obscures the wedge-shaped condensation funnel. The corresponding radar images in Figs. 11b and 11c show high Z_e and low ρ_{hv} at the tornado location, indicative of significant debris (see Schultz et al. 2012; Bodine et al. 2013). The inflow sector shows distinct bands of high and low Z_e values and a connection to a wider band of 50-dBZ echo extending southwest of the tornado location.

The Hackleburg storm affords an excellent opportunity to relate tornado severity to a significant thermal boundary. The Hackleburg tornado may be characterized as the most significant (in terms of *specific* DPI[7]) tornado of the day, since it produced extensive EF-5 damage [and had the greatest estimated wind speed of 210 miles per hour (mph) or 94 m s^{-1}], developed a swath width of 2.0 km, and

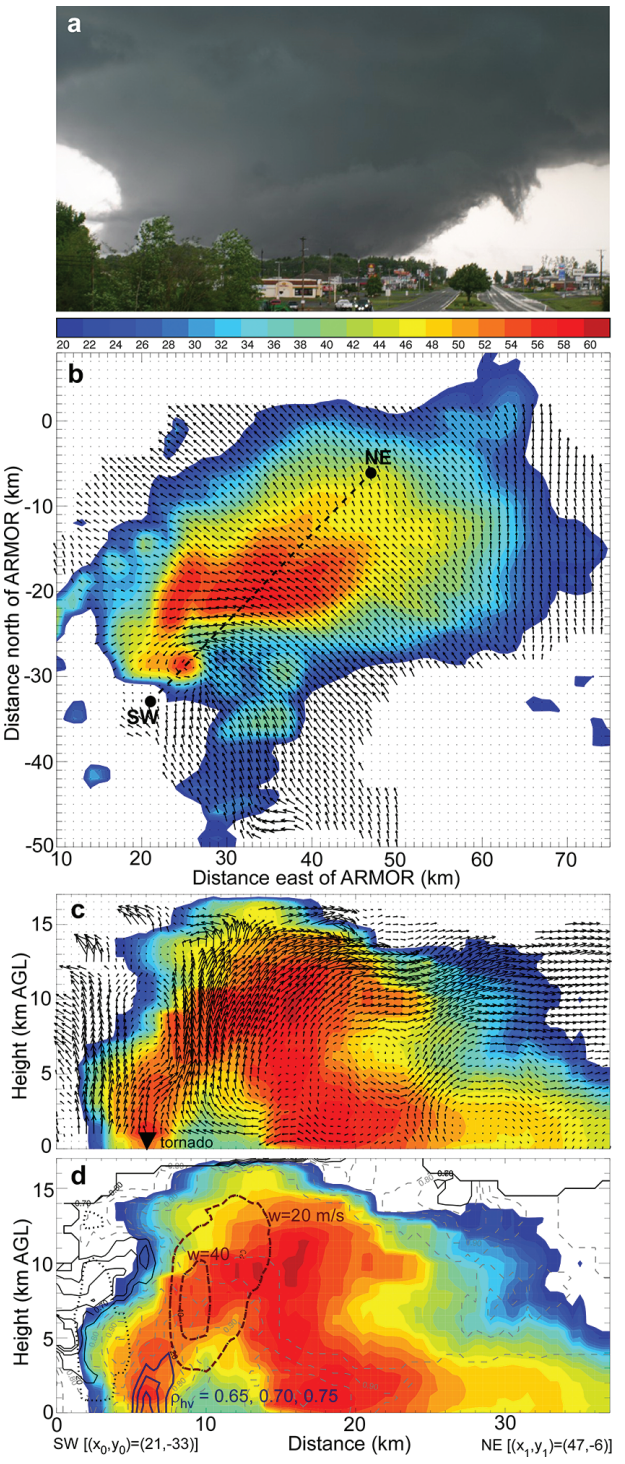

Fig. 10. (a) Image of the Cullman tornado near 2020 UTC, with a view toward the north-northwest (courtesy of C. Whisenant, *Arab Tribune*). (b) Horizontal section of storm-relative flow at 1-km AGL, retrieved from a preliminary dual-Doppler analysis using the ARMOR and KHTX WSR-88Ds at 2023 UTC. (c) Vertical section of storm-relative flow vectors and Z_e (shaded) along line southwest–northeast. The inverted triangle represents the approximate location of the tornado. (d) Z_e (shaded), correlation coefficient (light dashed lines, with solid black lines showing values of 0.65, 0.70, 0.75), and select updraft contours of 20 and 40 m s^{-1} (black dashed lines). Vertical sections shown in (c) and (d) are along the dashed line with end points southwest and northeast.

[7] The term "specific DPI" is defined as the destructive potential index for a specific tornado.

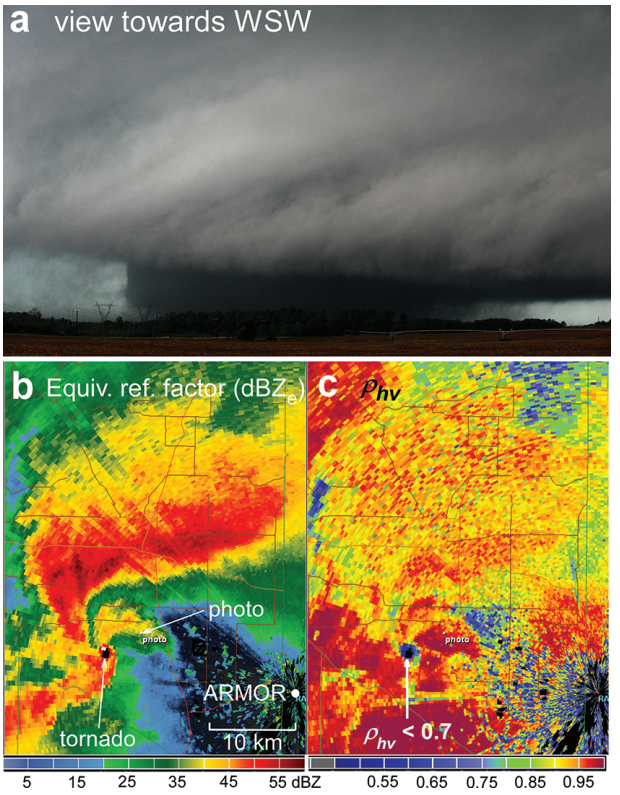

Fig. 11. (a) Image of the Hackleburg tornado at 2125 UTC (courtesy of Gary Cosby, *Decatur Daily*). Plan position indicator (PPI) images at 0.7° elevation angle of (b) Z_e and (c) ρ_{hv} from the ARMOR radar at 2121 UTC.

traveled the greatest distance (~212 km). This storm also developed supercell characteristics very quickly, within about 50 min of first echo. (A similar behavior was noted for the Moore, Oklahoma, tornado of 20 May 2013 by a reviewer of this manuscript.) The parent storm was also intense, as corroborated by very high total lightning flash rates (a peak value of about 21 flashes per square kilometer per 5-min interval) detected by the North Alabama Lightning Mapping Array (Goodman et al. 2005). Sequential surface plots like Fig. 8 indicate that the Hackleburg storm was in close proximity to the boundary (which was advancing slowly northward) at 2000 UTC, but then moved 10–20 km north on the cool side of the boundary during the remainder of its life cycle. The behavior of the Hackleburg storm and tornado appears to disagree with Nowotarski et al. (2011), who found that numerically simulated supercell storms over stable layers tend to exhibit lower vorticity near the surface. The low-level temperature profile of the sounding in Fig. 9 bears closest similarity to the 500-mb sounding in Nowotarski et al. (2011; Fig. 2), but the air is near saturation over the stable layer depth (Fig. 9) in contrast to much greater subsaturation within and 500 m above the stable layer in Nowotarski et al. They found that the 500-mb sounding was not conducive to the production of significant vertical vorticity at low levels. Further analysis of the Hackleburg storm (in progress) will perhaps provide further insight on this apparent difference. Nevertheless, this case provides an opportunity to build on less detailed observational studies (e.g., Maddox et al. 1980; Markowski et al. 1998; Rasmussen et al. 2000; King et al. 2003; Blanchard 2008) examining the interaction between thermal boundaries and supercell storms and the relationship to tornadogenesis.

The Tuscaloosa EF-4 tornado was well documented visually and on radar. Figure 12 presents an image of the tornado around 2212 UTC along with Z and V_r from KBMX at 2219 UTC. The radial velocity extremes across the circulation at a range of 63 km were at the maximum measured values around this time: the maximum outbound is 57 m s^{-1}, the maximum inbound is 72 m s^{-1} (161 mph), and the radial velocity difference is ΔV_r = 129 m s^{-1}. These values are quite high in view of the 63-km range (corresponding width of the beam is about 1 km) and sample height centered near 780 m AGL.[8] Figure 12a shows quasi-horizontal tubes along the right periphery (east flank) of the tornado as it demolished parts of Tuscaloosa. The horizontal tubes were common features associated with the Tuscaloosa, Cullman, and other violent tornadoes (see Fig. 10a) and are perhaps indicative of a large horizontal gradient in vertical motion along the edge of the tornadoes, as is apparent in the videos. Horizontal vortices (or appreciable horizontal vorticity) have been observed with Doppler radar by Bluestein et al. (2007) and Bluestein et al. (2012) and simulated by Lewellen et al. (2000, their Fig. 5).

Elsewhere, TN and GA experienced 71 and 13 tornadoes, respectively, some of which were produced by the Cullman, Cordova, and Tuscaloosa–Birmingham storms. In TN, significant tornadoes (three EF-4 and three EF-3) were confined to a relatively narrow corridor (Fig. 1), where 33 fatalities occurred. The other 57 tornadoes in TN were weak—EF-1 or EF-0. Over GA, the tornadoes were more broadly distributed. One EF-4 and four EF-3 tornadoes accounted for most of the 13 fatalities.

[8] For comparison, Lemon and Umscheid (2008) determined a ΔV_r of about 90 m s^{-1} in the EF-5 Greensburg (KS) tornado at a similar distance of 63 km. Tanamachi et al. (2012) provide additional details on polarimetric observations of this tornado.

EXAMPLES OF EXTREME DAMAGE FROM VIOLENT TORNADOES. In view of the large, long-tracked, and violent tornadoes that developed on 27 April 2011, it is worthwhile to summarize some descriptions of *extreme* damage. The following examples are taken from a longer list of noteworthy extreme tornado damage occurrences (McCaul et al. 2012):

- The EF-5 Smithville, MS, tornado carried a Ford Explorer (weight ~2.2 tons) about 900 m, where it impacted the Smithville water tower tank on the right edge of the tornado damage path.
- The first EF-5 tornado near Philadelphia, MS, stripped clumps of grass out by the roots, up to depths of 0.5 m, in addition to large sections of pavement stripped away from a roadway. Figure 13 shows a view of a tornado-plowed field, looking down track.
- The Tuscaloosa–Birmingham EF-4 tornado produced phenomenal damage northeast of Tuscaloosa (near the time of Figs. 12b and 12c), ripping several tapered railroad track steel truss towers (spanning a ravine) from their concrete foundations and lofting a 36-ton empty coal hopper rail car for 120 m.
- The Rainsville EF-5 tornado nearly completely eroded a mounded aboveground earthen storm shelter, where residents inside narrowly escaped severe injury or death.

POTENTIAL IMPORTANCE OF EXTERNAL INFLUENCES. This extensive outbreak presents an opportunity to further document external influences on tornadoes, such as gravity waves, thermal boundaries, and topography. The interaction between the thermal boundary and the Hackleburg storm was summarized in previous sections. The Cullman storm also quickly became tornadic after a prolonged development phase of 1.7 h (Table 2), and the tornado intensified rapidly as the parent supercell moved along the thermal boundary just before 2000 UTC (Fig. 8).

Gravity waves were sampled on the cool (stable) side of the thermal boundary (Fig. 9), where surface temperatures of ~17°C were maintained after the midday QLCS by persistent rain showers and cloud cover. Between 1855 and 1955 UTC, a packet of ducted gravity waves propagated over the MIPS site, producing significant surface pressure oscillations of about ±1 hPa that were correlated with wind fluctuations [consistent with the impedance relation as defined in Gossard and Hooke (1975) and refined by Coleman and Knupp (2010)] and laminar wave cloud

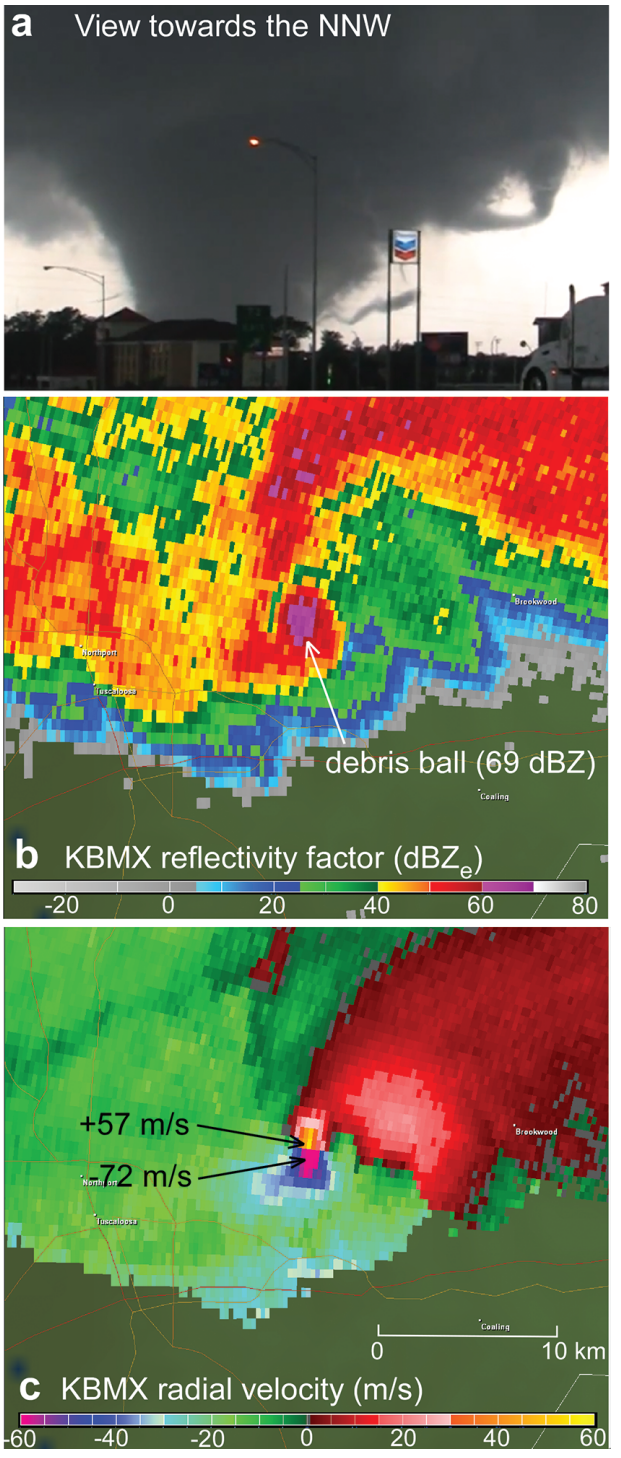

Fig. 12. (a) Image of the Tuscaloosa–Birmingham tornado over the city of Tuscaloosa at 2212 UTC (courtesy of Michael Wilhelm and John Brown). The view is toward the northwest. (b) PPI of equivalent reflectivity factor (Z_e) and radial velocity from the KBMX WSR-88D at 2219 UTC.

formations (Murphy et al. 2012). Since the waves moved directly over the MIPS site, the wave properties and boundary layer changes associated with the

Fig. 13. Example of extreme surface damage from the Philadelphia, MS, EF-5 tornado, in which grass and underlying soil were scoured up to 0.5 m deep by locally strong winds, possibly from "suction" vortices. The view is down track, toward the northeast. Photo copyright E. W. McCaul Jr., used with permission.

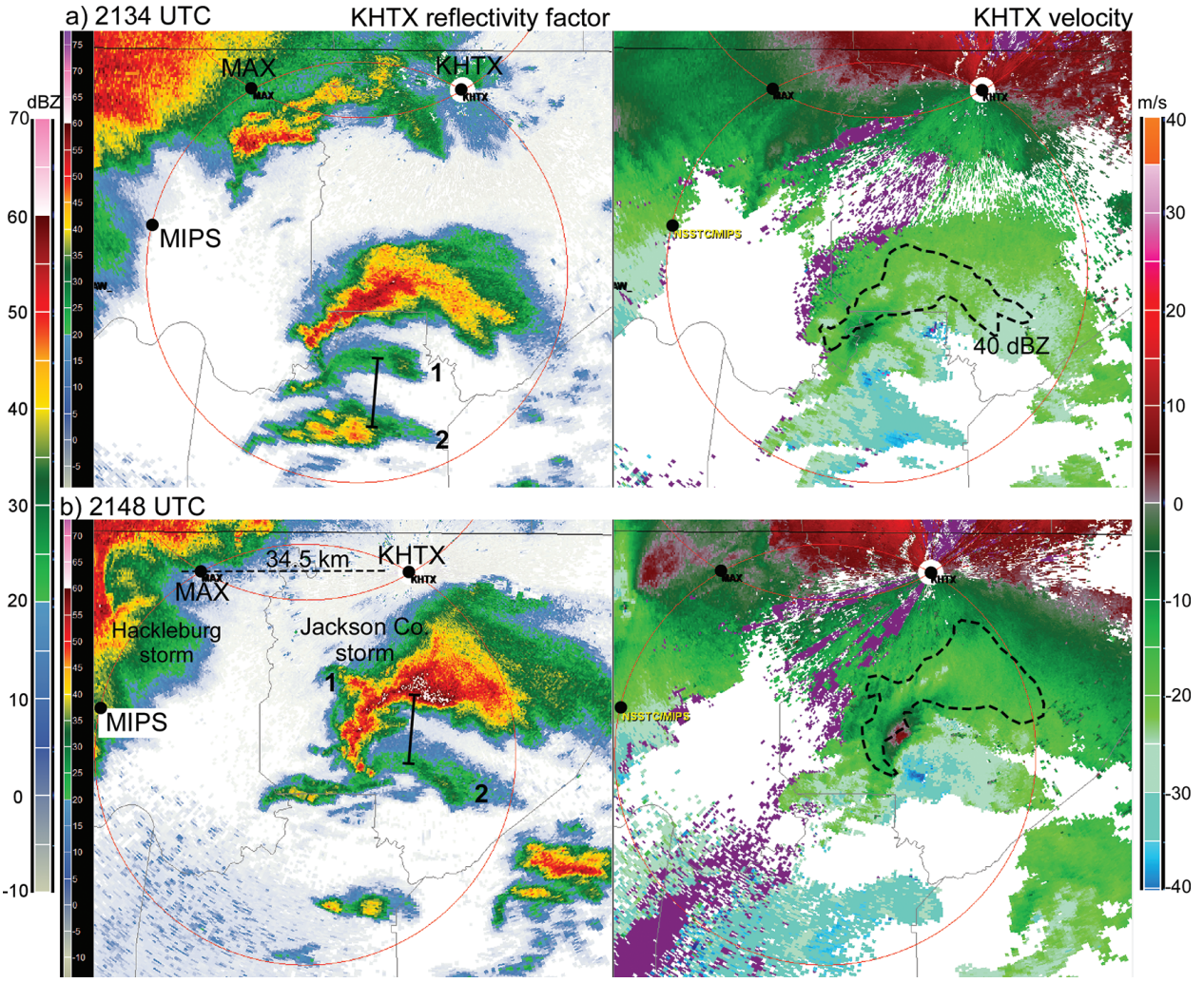

Fig. 14. Images of reflectivity factor and radial velocity of KHTX showing RS (labeled and 1 and 2) in relation to the development of the Jackson County storm. An EF-4 tornado formed after the two RSs intersected the developing supercell storm within a region of dual-Doppler coverage by the MAX and KHTX radars: (a) 2134 and (b) 2148 UTC.

wave passages were documented. After passing over the MIPS, the ducted gravity waves moved within the ARMOR–MAX–KHTX dual-Doppler region, allowing for a retrieval of the kinematic properties of the waves. The combination of MIPS and dual-Doppler data provides a comprehensive dataset on ducted gravity waves in a severe storms environment that will be presented in a future publication. An animation from the ARMOR radar (see online supplement) suggests a direct connection between the aforementioned waves and radar fine line features that intersected the Cullman storm (located near the thermal boundary) 40 km to the south.

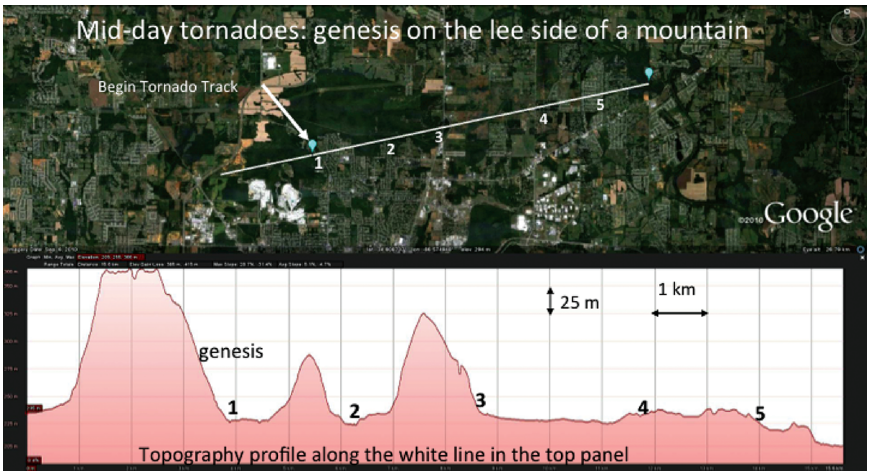

Fig. 15. Example of possible topographic influence on tornadogenesis and tornado intensity for an EF-1 tornado associated with the midday QLCS, 1659–1705 UTC. A detailed damage survey indicated that the tornado formed within the down-track side of Wade Mountain (point 1) and then exhibited well-defined areas of enhancements in damage within three downslope regions, labeled as 2, 3, 4, and 5.

In several instances, tornadogenesis corresponded to the merger of a RS with an existing mature or intensifying storm.[9] Figure 14 shows Z_e and V_r patterns where such an intersection occurred as two RSs (whose major axes are roughly perpendicular to the low-level shear), moving faster than the developing supercell storm and merged with it. During the merger of the second RS at 2148 UTC, the rotational velocity within the nascent supercell increased from about 7 m s^{-1} at 2134 to near 18 m s^{-1} at 2148 UTC, 17 min before tornadogenesis occurred. This pattern is consistent with that reported in Coleman and Knupp (2008). Because the merger event occurred within the dual-Doppler lobe formed by the MAX and KHTX radars (34-km baseline), the detailed kinematics of the RS and the response of the storm intersected by RS features can be examined.

We have noted that topographic variations frequently correlate with variations in tornado intensity, whereby tornado-scale vortices weaken while ascending a slope, and rapidly strengthen on the downslope side. This phenomenon was briefly discussed by Fujita (1974) for several tornadoes within the 3 April 1974 outbreak, Goodman and Knupp (1993) in their analysis of damage patterns produced by the F-4 Huntsville tornado on 15 November 1989, and Forbes (1998) for tornadoes in western Pennsylvania. Such a behavior has been recently simulated by Lewellen (2012). We have also noted (e.g., Coleman et al. 2010) that tornadogenesis may rapidly occur on the down-track side of ridges, as illustrated in Fig. 15 for one of the midday QLCS tornadoes. Damage from the tornado was first observed on the downslope side of Drake Mountain, indicated as location 1 in Fig. 15. A greater degree of damage, observed at four locations (2–5) along the track, corresponds to the downslope side of rather subtle topographic features, with the exception being location 4. Since many of the tornadoes in the outbreak passed over significant variations in topography, we are afforded the opportunity to substantiate and further quantify this behavior using the archive of detailed aerial imagery (30-cm resolution) available for this outbreak. In addition, several tornadoes formed in the rugged, tree-covered terrain of northeast AL and eastern AL during the afternoon outbreak, providing additional examples for further detailed analysis of tree fall patterns (e.g., Beck and Dotzek 2010; Godfrey and Peterson 2012; Karstens et al. 2013).

DISCUSSION AND CONCLUSIONS. The tornado outbreak of 27 April 2011 was an extreme weather disaster comparable to, and even surpassing,

[9] Scientific interest in mergers has increased in recent years (e.g., Lee et al. 2006). Several studies investigating merger events associated with tornadic storms were presented at the recent 26th Conference on Severe Local Storms in November 2012 (e.g., Rogers 2012; Hastings et al. 2012a,b).

the 3–4 April 1974 tornado outbreak. While the total number of tornadoes over a 24-h period (199) exceeded that in the April 1974 outbreak (148), the areal coverage of the 27 April outbreak was about 25% that of the 1974 outbreak, making the 2011 event very concentrated. Hence, the impact over the region affected (AL in particular) was substantial. We also note that tornado super outbreaks may significantly change short-term tornado climatologies, such as the study by Smith et al. (2012), which included the 2003–12 period.

Three rounds of contrasting mesoscale organization of deep convection occurred on 27 April, ranging from QLCSs to isolated supercell storms. In contrast, the 3 April 1974 outbreak exhibited linear arrangements of embedded or adjacent supercell storms (Corfidi et al. 2010). On 27 April an early morning cluster of meso-β-scale components coalesced over MS to form a long QLCS, within which two mesoscale vortices (MV1 and MV2) formed. Each MV was associated with significant numbers of tornadoes, including several EF-3 tornadoes with long and wide damage paths. In total, the early morning QLCS produced 76 tornadoes over MS, AL, TN, and GA. MV2 was very well sampled within a dual-Doppler domain, while over a dozen tornadoes were spawned within a 30-min period.

Following a midday QLCS that produced seven EF-0 to EF-1 tornadoes over northern AL, supercell storms developed during the afternoon hours in an extremely favorable environment, producing the majority of EF-3 to EF-5 tornadoes and associated

INITIAL INVESTIGATION OF SOCIETAL ASPECTS

To supplement ongoing work on the 27 April 2011 tornado warning response (e.g., Klockow et al. 2012), we sought to evaluate Emergency Management Agency (EMA) practices in place across north AL counties and establish a set of recommendations for improvements to weather threat communication. Procedures for weather warning information dissemination by EMAs vary greatly by county, most evident in outdoor warning siren use. Siren policy could play a significant role in shaping perceptions about warning information, as vast majorities of people receive warning information from sirens (NOAA 2009). Implementation of mass notification systems, such as a reverse 911 system, was also examined. Most EMA staff cited financial limitations, especially in counties with larger populations, and small staff size as inhibitors for employing these systems. Only one north AL county (DeKalb) has this type of system in place. The use of social media also varies greatly across county lines: some northern AL counties have no social media presence, but significant populations in other counties employ Facebook and/or Twitter accounts to provide status updates and threat information to residents and even take citizen reports of hazard (e.g., downed trees or power lines) locations. A consolidated list of recommendations (Mullins et al. 2012) was included in the Tornado Recovery Action Council of Alabama (TRAC) final report to the Alabama governor's office on how to better prepare and warn citizens of future severe weather hazards (TRAC 2012). Following the release of that report, a roundtable discussion on possible avenues for improving tornado warning dissemination was held at UAH. Participants included NWS forecasters, EMA personnel, severe weather researchers, social scientists, and local broadcast and private meteorologists. This meeting marked the beginning of increased integration among north AL weather and emergency professionals to effectively communicate hazard information to the public.

The intensity, duration, and scope of the outbreak created exceptional challenges for EMA offices, specifically widespread and long-lasting (> 5 days in many areas) power outages, which left residents with few if any sources of weather threat information or communication services and sharing of emergency response. Resource allocation as part of the North Alabama Mutual Aid Association (NAMAA) was complicated when emergency response personnel and equipment sent to aid response to storms earlier in the day were called back to their home counties in the midst of the evolving outbreak. Sharing emergency resources must be done with an understanding of the potential for new threats that change needs.

In addition to stresses on warning dissemination and response, perhaps another component of the tragically high death tolls involved the survivability of the event in the shelter that was available. The large number of violent tornadoes and relative lack of basements or below-ground shelters in most AL homes may have led to fatalities for individuals that sought shelter, but in a structure unable to survive the severity of violent tornadoes. Simmons and Sutter (2012b) evaluate this problem with statistical methods and show the high death tolls of 2011 (not just the 27 April event) were likely more due to the extreme nature of the 2011 outbreaks rather than only residents' high climatological and/or social tornado vulnerabilities. Still, they contend that this result does not indicate that social vulnerabilities had no effect. Marshall et al. (2012) show that construction practices along the path of the Tuscaloosa–Birmingham EF-4 were below optimal methods and resulted in higher damage amounts, and possibly higher death tolls, than may have occurred if more stringent construction techniques were used.

Significant tornado events are often followed by an "enhanced interest" in obtaining storm shelters and/or safe rooms (Simmons and Sutter 2012a), and in fact, over the last two years, shelter installation within both existing and newly constructed single family dwellings in north AL has risen dramatically and has been frequently used as an incentive in new home sales.

large numbers of fatalities (316), injuries (> 2700), and damage (~$11 billion). A very high fraction (~90%) of the supercell storms produced tornadoes within an environment very conducive to strong tornadoes.

One fundamental question posed by both physical and social scientists concerns the large number of fatalities (316 total; 238 in AL). A portion of the work summarized in the sidebar on "Initial investigation of societal aspects" highlighted inconsistencies and improvements needed in the warning dissemination process and progressed the interaction among north AL weather researchers, forecasters, social scientists, EMA personnel, and broadcasters with the goal of ensuring efficient and consistent weather threat communication to the public in the future.

Special datasets acquired within the outbreak region, and northern AL in particular, will afford opportunities to expand our understanding of physical processes of tornadogenesis and tornado maintenance produced within QLCSs and supercell storms. Specific research prospects include the following:

- A more detailed investigation of the kinematics of reflectivity segments, their relative frequency, and their potential importance in tornadogenesis. This work will provide further details on the physics of the interaction between RSs and supercell storms or QLCSs (Coleman and Knupp 2008; T. A. Murphy et al. 2013, unpublished manuscript).
- Examination of the time-evolving kinematics (vertical vorticity in particular) and tornadogenesis within a mature MV.
- Analysis of the rapid formation of cyclonic circulations along the leading edge of the midday QLCS.
- A close examination of debris transport and the relation to 3D flows within a long-lived supercell storm.
- A detailed analysis of the evolution of a baroclinic boundary and its impact on supercell storms, two of which spawned EF-5 tornadoes.
- The influence of topography on tornado-scale vortices, including apparent tornadogenesis, variations in intensity, and inferences on variations in the surface wind as inferred from tree fall patterns.

ACKNOWLEDGMENTS. A National Science Foundation Rapid Response Research Grant, AGS-1140387, provided funding for this initial research. Dr. Cody Kirkpatrick (Indiana University) generated the regional composite animation in Fig. ES1 (see online supplement). Dr. Chad Shafer (University of South Alabama) generously provided the N2 calculation shown in Table 1. We thank the numerous individuals who provided valuable information, including visual images and animations of many of the tornadoes on this day. This paper is dedicated to those who experienced loss of life, loved ones, property, and trauma on this fateful day.

REFERENCES

Andra, D. L., 1997: The origin and evolution of the WSR-88D mesocyclone recognition nomogram. Preprints, *28th Conf. on Severe Local Storms,* Austin, TX, Amer. Meteor. Soc., 364–365.

Atkins, N. T., and M. St. Laurent, 2009: Bow echo mesovortices. Part II: Their genesis. *Mon. Wea. Rev.,* **137,** 1514–1532, doi:10.1175/2008MWR2650.1.

Beck, V., and N. Dotzek, 2010: Reconstruction of near-surface tornado wind fields from forest damage. *J. Appl. Meteor. Climatol.,* **49,** 1517–1537, doi:10.1175/2010JAMC2254.1.

Birmingham News, cited 2011: Alabama tornadoes: Mountain of storm debris removed. [Available online at http://blog.al.com/spotnews/2011/05/alabama_tornadoes_mountain_of.html.]

Blanchard, D. O., 2008: Interactions between a supercell and a quasi-stationary frontal boundary. *Mon. Wea. Rev.,* **136,** 5199–5210, doi:10.1175/2008MWR2437.1.

Bluestein, H. B., C. C. Weiss, M. M. French, E. M. Holthaus, R. L. Tanamachi, S. Frasier, and A. L. Pazmany, 2007: The structure of tornadoes near Attica, Kansas, on 12 May 2004: High-resolution, mobile, Doppler radar observations. *Mon. Wea. Rev.,* **135,** 475–506, doi:10.1175/MWR3295.1.

——, J. C. Snyder, J. B. Houser, and A. L. Pazmany, 2012: Rapid-scan, polarimetric, Doppler-radar observations of an EF-5 tornado in Oklahoma on 24 May 2011. Preprints, *26th Conf. on Severe Local Storms,* Nashville, TN, Amer. Meteor. Soc., 16.3. [Available online at https://ams.confex.com/ams/26SLS/webprogram/Paper212022.html.]

Bodine, D. J., M. R. Kumjian, R. D. Palmer, P. L. Heinselman, and A. V. Ryzhkov, 2013: Tornado damage estimation using polarimetric radar. *Wea. Forecasting,* **28,** 139–158, doi:10.1175/WAF-D-11-00158.1.

Bosart, L. F., A. Seimon, K. D. LaPenta, and M. J. Dickinson, 2006: Supercell tornadogenesis over complex terrain: The Great Barrington, Massachusetts, tornado on 29 May 1995. *Wea. Forecasting,* **21,** 897–922, doi:10.1175/WAF957.1.

Brooks, H. E., 2004: On the relationship of tornado path length and width to intensity. *Wea. Forecasting,* **19,** 310–319, doi:10.1175/1520-0434(2004)0192.0.CO;2.

Bunkers, M. J., M. R. Hjelmfelt, and P. L. Smith, 2006a: An observational examination of long-lived supercells.

Part I: Characteristics, evolution, and demise. *Wea. Forecasting,* **21,** 673–688, doi:10.1175/WAF949.1.

——, J. S. Johnson, L. J. Czepyha, J. M. Grzywacz, B. A. Klimowski, and M. R. Hjelmfelt, 2006b: An observational examination of long-lived supercells. Part II: Environmental conditions and forecasting. *Wea. Forecasting,* **21,** 689–714, doi:10.1175/WAF952.1.

Coleman, T. A., and K. R. Knupp, 2008: The interactions of gravity waves with mesocyclones: Preliminary observations and theory. *Mon. Wea. Rev.,* **136,** 4206–4219, doi:10.1175/2008MWR2391.1.

——, and ——, 2010: A nonlinear impedance relation for the surface winds in pressure disturbances. *J. Atmos. Sci.,* **67,** 3409–3422, doi:10.1175/2010JAS3457.1.

——, C. C. Crowe, and K. Knupp, 2010: Mesoscale phenomena affecting the AL EF-4 tornadoes during the Super Tuesday outbreak of 5–6 February 2008. Preprints, *24th Conf. on Severe Local Storms,* Savannah, GA, Amer. Meteor. Soc., 3A.3. [Available online at https://ams.confex.com/ams/24SLS/webprogram/Paper142202.html.]

Corfidi, S. F., S. J. Weiss, J. S. Kain, S. J. Corfidi, R. M. Rabin, and J. J. Levit, 2010: Revisiting the 3–4 April 1974 super outbreak of tornadoes. *Wea. Forecasting,* **25,** 465–510, doi:10.1175/2009WAF2222297.1.

Davies, J. M., C. A. Doswell, D. W. Burgess, and J. F. Weaver, 1994: Some noteworthy aspects of the Hesston, Kansas, tornado family of 13 March 1990. *Bull. Amer. Meteor. Soc.,* **75,** 1007–1017, doi:10.1175/1520-0477(1994)0752.0.CO;2.

Dial, G. L., J. P. Racy, and R. L. Thompson, 2010: Short-term convective mode evolution along synoptic boundaries. *Wea. Forecasting,* **25,** 1430–1446, doi:10.1175/2010WAF2222315.1.

Doswell, C. A., R. Edwards, R. L. Thompson, J. A. Hart, and K. C. Crosbie, 2006: A simple and flexible method for ranking severe weather events. *Wea. Forecasting,* **21,** 939–951, doi:10.1175/WAF959.1.

Forbes, G. S., 1998: Topographic influences on tornadoes in Pennsylvania. Preprints, *19th Conf. on Severe Local Storms,* Minneapolis, MN, Amer. Meteor. Soc., 269–272.

Fujita, T. T., 1974: Jumbo tornado outbreak of 3 April 1974. *Weatherwise,* **27,** 116–126, doi:10.1080/00431672.1974.9931693.

Godfrey, C. M., and C. J. Peterson, 2012: Reconstruction of near-surface tornado wind fields from forest damage patters in complex terrain. Preprints, *26th Conf. on Severe Local Storms,* Nashville, TN, Amer. Meteor. Soc., 115. [Available online at https://ams.confex.com/ams/26SLS/webprogram/Paper215087.html.]

Goodman, S., and K. R. Knupp, 1993: Tornadogenesis via squall line and supercell interaction: The 15 November 1989 Huntsville tornado. *The Tornado: Its Structure, Dynamics Prediction and Hazards, Geophys. Monogr.,* Vol. 79, Amer. Geophys. Union, 183–200.

——, and Coauthors, 2005: The North Alabama Lightning Mapping Array: Recent severe storm observations and future prospects. *Atmos. Res.,* **76,** 423–437, doi:10.1016/j.atmosres.2004.11.035.

Grams, J. S., R. L. Thompson, D. V. Snively, J. A. Prentice, G. M. Hodges, and L. J. Reames, 2012: A climatology and comparison of parameters for significant tornado events in the United States. *Wea. Forecasting,* **27,** 106–123, doi:10.1175/WAF-D-11-00008.1.

Hastings, R. M., Y. P. Richardson, and P. Markowski, 2012a: Mergers in supercell environments. Part II: Tornadogenesis potential during merger as evaluated by changes in the near-surface low-level mesocyclone. Preprints, *26th Conf. on Severe Local Storms,* Nashville, TN, Amer. Meteor. Soc., 143. [Available online at https://ams.confex.com/ams/26SLS/webprogram/Paper212524.html.]

——, ——, ——, J. Wurman, and C. C. Weiss, 2012b: Mergers in supercell environments. Part I: Conceptual models of mechanisms governing merger outcomes. Preprints, *26th Conf. on Severe Local Storms,* Nashville, TN, Amer. Meteor. Soc., 11B.6. [Available online at https://ams.confex.com/ams/26SLS/webprogram/Paper212519.html.]

Karstens, C. D., W. A. Gallus, B. D. Lee, and C. A. Finley, 2013: Analysis of tornado-induced tree fall using aerial photography from the Joplin, Missouri, and Tuscaloosa-Birmingham, Alabama, tornadoes of 2011. *J. Appl. Meteor. Climatol.,* **52,** 1049–1068, doi:10.1175/JAMC-D-12-0206.1.

King, P., M. J. Leduc, D. Sills, N. R. Donaldson, D. R. Hudak, P. Joe, and B. P. Murphy, 2003: Lake breezes in southern Ontario and their relation to tornado climatology. *Wea. Forecasting,* **18,** 795–807, doi:10.1175/1520-0434(2003)0182.0.CO;2.

Klockow, K. E., R. McPherson, A. Tarhule, H. Brooks, and R. P. Thomas, 2012: How forecast and warning did, and did not, shape response in the April 27, 2011 tornado outbreak. Preprints, *Special Symp. on Tornado Disasters of 2011,* New Orleans, LA, Amer. Meteor. Soc., J2.5. [Available online at https://ams.confex.com/ams/92Annual/webprogram/Paper202675.html.]

Knox, J. A., and Coauthors, 2013: Tornado debris characteristics and trajectories during the 27 April 2011 super outbreak as determined using social media data. *Bull. Amer. Meteor. Soc.,* **94,** 1371–1380, doi:10.1175/BAMS-D-12-00036.1.

Koch, S. E., D. Hamilton, D. Cramer, and A. Langmaid, 1998: Mesoscale dynamics in the Palm Sunday

tornado outbreak. *Mon. Wea. Rev.,* **126,** 2031–2060, doi:10.1175/1520-0493(1998)1262.0.CO;2.

Langmaid, A. H., and A. J. Riordan, 1998: Surface mesoscale processes during the 1994 Palm Sunday tornado outbreak. *Mon. Wea. Rev.,* **126,** 2117–2132, doi:10.1175/1520-0493(1998)1262.0.CO;2.

Lee, B. D., B. F. Jewett, and R. B. Wilhelmson, 2006: The 19 April 1996 Illinois tornado outbreak. Part I: Cell evolution and supercell isolation. *Wea. Forecasting,* **21,** 433–448, doi:10.1175/WAF944.1.

Lemon, L. R., and M. Umscheid, 2008: The Greensburg, KS tornadic storm: A storm of extremes. Preprints, *24th Conf. on Severe Local Storms,* Savannah, GA, Amer. Meteor. Soc., 2.4. [Available online at https://ams.confex.com/ams/24SLS/webprogram/Paper141811.html.]

Lewellen, D. C., 2012: Effects of topography on tornado dynamics: A simulation study. Preprints, *26th Conf. on Severe Local Storms,* Nashville, TN, Amer. Meteor. Soc., 4B.1. [Available online at https://ams.confex.com/ams/26SLS/webprogram/Paper211460.html.]

——, W. S. Lewellen, and J. Xia, 2000: The influence of a local swirl ratio on tornado intensification near the surface. *J. Atmos. Sci.,* **57,** 527–544, doi:10.1175/1520-0469(2000)0572.0.CO;2.

Maddox, R. A., L. R. Hoxit, and C. F. Chappell, 1980: A study of tornadic thunderstorm interactions with thermal boundaries. *Mon. Wea. Rev.,* **108,** 322–336, doi:10.1175/1520-0493(1980)1082.0.CO;2.

Magsig, M. A., and J. T. Snow, 1998: Long-distance debris transport by tornadic thunderstorms. Part I: The 7 May 1995 supercell thunderstorm. *Mon. Wea. Rev.,* **126,** 1430–1449, doi:10.1175/1520-0493(1998)1262.0.CO;2.

Markowski, P. M., E. N. Rasmussen, and J. M. Straka, 1998: The occurrence of tornadoes in supercells interacting with boundaries during VORTEX-95. *Wea. Forecasting,* **13,** 852–859, doi:10.1175/1520-0434(1998)0132.0.CO;2.

Marshall, T. P., J. Stefkovich, J. DeBlock, J. G. Ladue, and C. Karstens, 2012: Damage survey of the Tuscaloosa-Birmingham tornado on 27 April 2011. Preprints, *26th Conf. on Severe Local Storms,* Nashville, TN, Amer. Meteor. Soc., 5.3. [Available online at https://ams.confex.com/ams/26SLS/webprogram/Paper211667.html.]

McCaul, E. W., Jr., K. Knupp, C. B. Darden, and K. B. Laws, 2012: Extreme damage incidents in the 27 April 2011 tornado super outbreak. Preprints, *26th Conf. on Severe Local Storms*, Nashville, TN, Amer. Meteor. Soc., 114. [Available online at https://ams.confex.com/ams/26SLS/webprogram/Paper212695.html.]

Mercer, A. E., C. E. Shafer, C. A. Doswell, L. M. Leslie, and M. B. Richman, 2012: Synoptic composites of tornadic and nontornadic outbreaks. *Mon. Wea. Rev.,* **140,** 2590–2608, doi:10.1175/MWR-D-12-00029.1.

Mullins, S. A., E. V. Schultz, K. Knupp, and K. Klockow, 2012: Public perception and response to severe weather: Lessons from the 27 April 2011 tornado outbreak across N Alabama. Preprints, *Special Symp. on the Tornado Disasters of 2011,* New Orleans, LA, Amer. Meteor. Soc., 638. [Available online at https://ams.confex.com/ams/92Annual/webprogram/Paper197896.html.]

Murphy, T. A., T. A. Coleman, and K. R. Knupp, 2012: Observations and analysis of atmospheric waves during the historic April 27, 2011 tornado outbreak. Preprints, *26th Conf. on Severe Local Storms,* Nashville, TN, Amer. Meteor. Soc., 107. [Available online at https://ams.confex.com/ams/26SLS/webprogram/Paper212024.html.]

NOAA, 2009: Service assessment: Super Tuesday tornado outbreak of February 5–6, 2008. U.S. Department of Commerce/NOAA/NWS Rep., 48 pp. [Available online at www.nws.noaa.gov/os/assessments/pdfs/super_tuesday.pdf.]

——, 2011: Service assessment: The historic tornadoes of April 2011. U.S. Department of Commerce/NOAA/NWS Rep., 76 pp. [Available online at www.nws.noaa.gov/os/assessments/pdfs/historic_tornadoes.pdf.]

——, cited 2012: 2011 tornado information. [Available online at www.noaanews.noaa.gov/2011_tornado_information.html.]

Nowotarski, C. J., P. M. Markowski, Y. P. Richardson, 2011: The characteristics of numerically simulated supercell storms situated over statically stable boundary layers. *Mon. Wea. Rev.,* **139,** 3139–3162.

Rasmussen, E. N., 2003: Refined supercell and tornado parameters. *Wea. Forecasting,* **18,** 530–535, doi:10.1175/1520-0434(2003)182.0.CO;2.

——, S. Richardson, J. M. Straka, P. M. Markowski, and D. O. Blanchard, 2000: The association of significant tornadoes with a baroclinic boundary on 2 June 1995. *Mon. Wea. Rev.,* **128,** 174–191, doi:10.1175/1520-0493(2000)1282.0.CO;2.

Rogash, J. A., and R. D. Smith, 2000: Multiscale overview of a violent tornado outbreak with attendant flash flooding. *Wea. Forecasting,* **15,** 416–431, doi:10.1175/1520-0434(2000)0152.0.CO;2.

Rogers, J. W., 2012: Significant tornado events associated with cell mergers. Preprints, *26th Conf. on Severe Local Storms,* Nashville, TN, Amer. Meteor. Soc., 9.4. [Available online at https://ams.confex.com/ams/26SLS/webprogram/Paper211575.html.]

Ryzhkov, A. V., T. J. Schuur, D. W. Burgess, and D. S. Zrnic, 2005: Polarimetric tornado detection. *J. Appl. Meteor.,* **44,** 557–570, doi:10.1175/JAM2235.1.

Schenkman, A. D., M. Xue, A. Shapiro, K. Brewster, and J. Gao, 2011a: The analysis and prediction of the 8–9 May 2007 Oklahoma tornadic mesoscale convective system by assimilating WSR-88D and CASA radar data using 3DVAR. *Mon. Wea. Rev.,* **139,** 224–246, doi:10.1175/2010MWR3336.1.

——, ——, ——, ——, and ——, 2011b: Impact of CASA radar and Oklahoma mesonet data assimilation on the analysis and prediction of tornadic mesovortices in an MCS. *Mon. Wea. Rev.,* **139,** 3422–3445, doi:10.1175/MWR-D-10-05051.1.

——, ——, and ——, 2012: Tornadogenesis in a simulated mesovortex within a mesoscale convective system. *J. Atmos. Sci.,* **69,** 3372–3390, doi:10.1175/JAS-D-12-038.1.

Schultz, C. J., and Coauthors, 2012: Dual-polarization tornadic debris signatures. Part I: Examples and utility in an operational setting. *Electron. J. Oper. Meteor.,* **13,** 120–137.

Shafer, C. M., and C. A. Doswell III, 2010: A multivariate index for ranking and classifying severe weather outbreaks. *Electron. J. Severe Storms Meteor.,* **5,** 1–39.

——, A. E. Mercer, M. B. Richman, L. M. Leslie, and C. A. Doswell, 2012: An assessment of areal coverage of severe weather parameters for severe weather outbreak diagnosis. *Wea. Forecasting,* **27,** 809–831, doi:10.1175/WAF-D-11-00142.1.

Simmons, K. M., and D. Sutter, 2012a: The 2011 tornadoes and the future of tornado research. *Bull. Amer. Meteor. Soc.,* **93,** 959–961, doi:10.1175/BAMS-D-11-00126.1.

——, and ——, 2012b: *Deadly Season: Analysis of the 2011 Tornado Outbreaks.* Amer. Meteor. Soc., 103 pp.

——, ——, and R. Pielke, 2012: Blown away: Monetary and human impacts of the 2011 U.S. tornadoes. Extreme events and insurance: 2011 annus horribilis, C. Courbage and W.R. Stahel, Eds., The Geneva Association Rep., 107–120. [Available online at www.genevaassociation.org/media/200995/GA-2012-Geneva_report%5B5%5D.pdf.]

Smith, B. T., R. L. Thompson, J. S. Grams, C. Broyles, and H. E. Brooks, 2012: Convective modes for significant severe thunderstorms in the contiguous United States. Part I: Storm classification and climatology. *Wea. Forecasting,* **27,** 1114–1135, doi:10.1175/WAF-D-11-00115.1.

Tanamachi, R. L., H. B. Bluestein, J. B. Houser, S. J. Frasier, and K. M. Hardwick, 2012: Mobile, X-band, polarimetric Doppler radar observations of the 4 May 2007 Greensburg, Kansas tornadic supercell. *Mon. Wea. Rev.,* **140,** 2103–2125, doi:10.1175/MWR-D-11-00142.1.

Thompson, R. L., and M. D. Vescio, 1998: The destruction potential index: A method for comparing tornado days. Preprints, *19th Conf. on Severe Local Storms*, Minneapolis, MN, Amer. Meteor. Soc., 280–282.

——, and R. Edwards, 2000: An overview of the environmental conditions and forecast implications of the 3 May 1999 tornado outbreak. *Wea. Forecasting,* **15,** 682–699, doi:10.1175/1520-0434(2000)0152.0.CO;2.

——, ——, J. A. Hart, K. L. Elmore, and P. Markowski, 2003: Close proximity soundings within supercell environments obtained from the Rapid Update Cycle. *Wea. Forecasting,* **18,** 1243–1261, doi:10.1175/1520-0434(2003)0182.0.CO;2.

——, C. M. Mead, and R. Edwards, 2007: Effective storm-relative helicity and bulk shear in supercell thunderstorm environments. *Wea. Forecasting,* **22,** 102–115, doi:10.1175/WAF969.1.

——, B. T. Smith, J. S. Grams, A. R. Dean, and C. Broyles, 2012: Convective modes for significant severe thunderstorms in the contiguous United States. Part II: Supercell and QLCS tornado environments. *Wea. Forecasting,* **27,** 1136–1154, doi:10.1175/WAF-D-11-00116.1.

TRAC, 2012: Cultivating a state of readiness: Our response to April 27, 2011. Tornado Recovery Action Council (TRAC) of Alabama Rep., 117 pp. [Available online at http://tracAL.org/wp-content/uploads/2012/01/TRAC_Report.pdf.]

Trapp, R. J., and M. L. Weisman, 2003: Low-level mesovortices within squall lines and bow echoes. Part II: Their genesis and implications. *Mon. Wea. Rev.,* **131,** 2804–2823, doi:10.1175/1520-0493(2003)1312.0.CO;2.

——, G. J. Stumpf, and K. L. Manross, 2005a: A reassessment of the percentage of tornadic mesocyclones. *Wea. Forecasting,* **20,** 680–687, doi:10.1175/WAF864.1.

——, S. A. Tessendorf, E. S. Godfrey, and H. E. Brooks, 2005b: Tornadoes from squall lines and bow echoes. Part I: Climatological distribution. *Wea. Forecasting,* **20,** 23–33, doi:10.1175/WAF-835.1.

Weisman, M. A., and R. J. Trapp, 2003: Low-level mesovortices within squall lines and bow echoes. Part I: Overview and dependence on environmental shear. *Mon. Wea. Rev.,* **131,** 2779–2803, doi:10.1175/1520-0493(2003)1312.0.CO;2.

——, C. Evans, and L. Bosart, 2013: The 8 May 2009 superderecho: Analysis of a real-time explicit forecast. *Wea. Forecasting,* **28,** 863–892, doi:10.1175/WAF-D-12-00023.1.